Inner retinal preservation in rat models of retinal degeneration implanted with subretinal photovoltaic arrays

Jacob G. Light[a,b], James W. Fransen[c], Adewumi N. Adekunle[a], Alice Adkins[b], Gobinda Pangeni[d], James Loudin[e], Keith Mathieson[e,g], Daniel V. Palanker[e,f], Maureen A. McCall[c,d], Machelle T. Pardue[a,b].

[a]Ophthalmology, Emory University; [b]Rehab R&D Center of Excellence, Atlanta VA Medical Center; [c]Anatomical Sciences & Neurobiology, [d]Ophthalmology & Visual Sciences, University of Louisville; [e]Hansen Experimental Physics Laboratory, [f]Ophthalmology, Stanford University; [g]Institute of Photonics, University of Strathclyde, UK

Corresponding Author:

Machelle T. Pardue, PhD
Research Service (151Oph)
Atlanta VA Medical Center
1670 Clairmont Rd
Decatur, GA 30033

Ph: 404-321-6111 x7342
Fax: 404-728-4847
mpardue@emory.edu

Abstract:

Photovoltaic arrays (PVA) implanted into the subretinal space of patients with retinitis pigmentosa (RP) are designed to electrically stimulate the remaining inner retinal circuitry in response to incident light, thereby recreating a visual signal when photoreceptor function declines or is lost. Preservation of inner retinal circuitry is critical to the fidelity of this transmitted signal to ganglion cells and beyond to higher visual targets. Post-implantation loss of retinal interneurons or excessive glial scarring could diminish and/or eliminate PVA-evoked signal transmission. As such, assessing the morphology of the inner retina in RP animal models with subretinal PVAs is an important step in defining biocompatibility and predicting success of signal transmission. In this study, we used immunohistochemical methods to qualitatively and quantitatively compare inner retinal morphology after the implantation of a PVA in two RP models: the Royal College of Surgeons (RCS) or transgenic S334ter-line 3 (S334ter-3) rhodopsin mutant rat. Two PVA designs were compared. In the RCS rat, we implanted devices in the subretinal space at 4 weeks of age and histologically examined them at 8 weeks of age and found inner retinal morphology preservation with both PVA devices. In the S334ter-3 rat, we implanted devices at 6 to 12 weeks of age and again, inner retinal morphology was generally preserved with either PVA design 16 to 26 weeks post implantation. Specifically, the length of rod bipolar cells and numbers of cholinergic amacrine cells were maintained along with their characteristic inner plexiform lamination patterns. Throughout the implanted retinas we found nonspecific glial reaction, but none showed additional glial scarring at the implant site. Our results indicate that subretinally implanted PVAs are well-tolerated in rodent RP models and that the inner retinal circuitry is preserved, consistent with our published results showing implant-evoked signal transmission.

Keywords: retina, prosthetic, bipolar cells, amacrine cells, Müller glial cells

1. Introduction

Retinitis pigmentosa (RP) and age-related macular degeneration (AMD) are leading causes of irreversible blindness worldwide (Hartong et al., 2006). In these diseases, vision loss, regardless of underlying etiology, results from degeneration of retinal photoreceptors. Remodeling of the inner retina occurs in late stages of disease (Jones and Marc, 2005; Marc and Jones, 2003; Marc et al., 2007; Strettoi et al., 2002), but photoreceptor degeneration leaves the neurons and circuitry of the inner retina relatively intact for extended periods of time (Humayun et al., 1999; Jones et al., 2003; Marc and Jones, 2003; Marc et al., 2007; Strettoi et al., 2002; Strettoi et al., 2003).

One promising approach that targets the remaining retinal circuitry to restore lost vision uses prosthetic devices to functionally replace photoreceptors. Several different designs and placement strategies are currently being evaluated. Epiretinal placement and stimulation of the retinal ganglion cells (RGC) should require algorithms to selectively achieve information transmission (Jensen et al., 2005; Humayun et al., 2012). Suprachoroidal implants (Cicione et al., 2012; Kanda et al., 2004; Morimoto et al., 2011; Wong et al., 2009; Yamauchi et al., 2005) and subretinal microphotodiode arrays (Chow et al., 2001; Mathieson et al., 2012; Rizzo, 2011; Zrenner et al., 1999) are designed to directly stimulate bipolar cells and theoretically utilize network-mediated retinal stimulation, preserving the integrative properties of second order neurons in the inner plexiform layer (IPL) (Asher et al., 2007; Wang et al., 2012). Other strategies utilize optogenetics to confer light sensitivity to bipolar or RGCs (Bi et al., 2006; Busskamp et al., 2012; Garg and Federman, 2013; Isago et al., 2012; Lin et al., 2008; Tomita et al., 2007) to directly stimulate retinal tissues.

Subretinally placed photovoltaic arrays (PVAs) provide targeted stimulation to the inner nuclear layer (INL) (Fransen et al., 2014) due to their current density distribution and size

(Mathieson et al. 2012). Because bipolar cells are interneurons that connect photoreceptors to RGCs they are involved in signal transmission with PVAs. Retention of these cells and formation of a functional retinal-prosthetic interface would aid in visual restoration. For this to occur there must be a high level of biocompatibility between the retina and prosthesis. As such, measures of the integrity of the bipolar cells and other retinal constituents are critical components to the evaluation of the success of any subretinal prosthetic.

Previous studies have attempted to characterize the condition of implanted and/or electrically stimulated retinal tissue histologically and immunohistochemically (Alamusi et al., 2013; Chow et al., 2001; Pardue et al., 2001; Ray et al., 2009; Ray et al., 2011; Tamaki et al., 2008). However, many of these studies have examined the effects only of certain aspects of the treatment paradigm, such as acute electrical stimulation or biocompatibility of a prosthetic device in wild-type animals that do not exhibit degenerative pathology. In this study, we examined retinal morphology after implantation of two generations of subretinal silicon devices in two RP rat models. We compared a monopolar PVA (mPVA) with no perforations (Chow et al., 2001) to a bipolar PVA (bPVA), which includes bipolar pixels separated by 5 μm gaps (Mathieson et al., 2012). Photovoltaic pixels in monopolar devices have individual active electrodes, but share a common large return electrode on the back side of the implant. Bipolar pixels are composed of 3 photodiodes in series, connected between the active electrode in the center of the pixel and a return electrode surrounding each pixel (Mathieson et al., 2012). All devices in the present study were photoactive. The bPVA gaps enhance proximity of the electrodes to inner retinal neurons and allow diffusion of extracellular milieu through the implant (Adkins et al., 2013; Mathieson et al., 2012). Since the subretinal PVA stimulates retinal neurons that are within close proximity to the electrode (Fransen et al., 2014), we focused our analysis on inner retinal cells that are likely activated by the PVA device. Rod bipolar cells and cholinergic amacrine cells represent well defined populations of cells with robust cellular

markers to assess overall inner retinal health. We also assessed glial reaction in tissues within and distal to the implant site from 16 to 26 weeks post implantation in the S334ter-3 and 4 weeks post implantation in the RCS rat. Our results suggest that both the mPVA and bPVA designs are well tolerated and preserve the necessary inner retinal circuitry that underlie the transmission of signals to the RGCs and beyond (Fransen et al., 2014).

2. Methods

2.1 Animals and Experimental Groups

All animal procedures were approved by the Institutional Animal Care and Use Committee and conformed to the ARVO Statement for the Use of Animals in Ophthalmology and Vision Research. Two models of RP were used: the Royal College of Surgeons (RCS) and S334ter-3 rats from an in-house breeding colony originated from breeders donated by Dr. Matthew LaVail (University of California, San Francisco) (LaVail et al., 1975; Mullen and LaVail, 1976).

The RCS rats (n=4) were implanted binocularly at 4 weeks of age and terminated 4 weeks post-implantation. RCS rats exhibit a moderate rate of photoreceptor degeneration; approximately 50% of the initial ONL thickness was present at the age of implantation (LaVail and Battelle, 1975). Four eyes were implanted with an mPVA device and 4 with a bPVA device. The eyes were divided such that all bPVA-implanted eyes were processed as frozen sections for retinal cross-sections and half the mPVA eyes processed similarly with the remaining prepared as retinal flat mounts.

S334ter-3 rats were implanted monocularly (right eye) with either an mPVA (n=4) or a bPVA (n=7) from 6 to 12 weeks of age and were terminated at 22 to 32 weeks of age (16-26 weeks of implantation). Monocular implantation accommodated superior colliculus recordings that are reported elsewhere (Fransen et al., 2014). The S334ter-3 is a rapid degeneration model

and most photoreceptors had degenerated at the time of implantation (McGill et al., 2012). All S334ter-3 eyes were processed as frozen sections. Additional cross sections were analyzed from three age-matched unimplanted control eyes from each RP strain, as well as 3 eyes from 8-week-old Long Evans wild-type rats acquired from Charles River.

2.2 Overview of Devices

Two types of PVA were explored: mPVA and bPVA (Mathieson et al., 2012; Pardue et al., 2005b). mPVA devices, provided by Optobionics, Inc (Glen Ellyn, IL), were fabricated using previously described thin-film fabrication methods (Chow et al., 2001). The mPVA is a 1 mm diameter silicon disk, 25 μm thick, containing 1200 microphotodiodes with active electrodes on one face and a common return electrode on the back, both coated with iridium oxide (Chow et al., 2001). The bPVA device's photovoltaic arrays were composed of triple-diode pixels fabricated on a silicon wafer. Each pixel contains an active electrode in its center and a return electrode at the circumference. Upon illumination with a pulse of light, each pixel generates a bi-phasic pulse of electric current flowing through the tissue between electrodes, primarily stimulating the inner nuclear layer (INL) cells (Fransen et al., 2014). Electrodes were coated in iridium oxide and the details of manufacturing methods of the bPVA were published previously (Wang et al., 2012). Five-μm wide gaps were etched between adjacent pixels for electrical isolation and to improve nutrients flow through the implant (Mathieson, et al. 2012). The bPVA device measured 0.8 x 1.2 mm and was 30-μm thick. bPVA devices were left in retinal tissue for histological analysis due to tissue destruction caused by removal.

2.3 Surgical Procedure

The surgical methods employed for implantation of the PVAs into the subretinal space have been described previously (Pardue et al., 2005b). Briefly, rats were anesthetized

[ketamine (60 mg/kg) and xylazine (7.5 mg/kg)] and placed into a sterile field. A traction suture was made at the superior limbus and the eye was rotated inferiorly. A ~1.0 mm incision was made in the superior globe reaching the vitreous. The eye was hydrated with a drop of saline, and a 10 minute waiting period was observed which allowed the retina to detach from the RPE. The PVA was then slid into the subretinal space with the electrodes in contact with the retina. Successful subretinal placement was confirmed via fundus examination and subsequent spectral domain-ocular coherence tomography (SD-OCT) imaging (Heidelberg HRA+OCT, Carlsbad, CA) (Fransen et al., 2014). Implants rested in the superior-temporal retina from 0.5 to 1 mm from the optic nerve head.

2.4 Immunohistochemistry

2.4.1 Cross-sections

Following anesthesia [ketamine (60 mg/kg)/xylazine (7.5 mg/kg)] and sacrifice [390 mg/mL pentobarbital sodium (Euthasol, Virbac AH, Inc., Fort Worth, TX)], eyes were immediately enucleated and fixed in 4% paraformaldehyde for 30 minutes. The posterior eyecup was bisected in the superior/inferior plane near the optic nerve, ensuring that the entire implant was intact and present in only one of the two resulting halves (Figure 1A). mPVA devices were gently extracted from the subretinal space using hydrodissection. bPVAs, which contain gaps through which the retinal tissue migrates (Palanker et al., 2004), were left in place to preserve retinal morphology around the implant. The tissue was cryoprotected overnight in 30% sucrose in 0.1M PBS and frozen in embedding medium (O.C.T. Tissue-Tek®, Sakura Finetek, Tokyo). Retinal sections in the superior/inferior plane (20-30 μm) were cut on a cryostat and thaw-mounted on glass slides. Sections containing the implant site were mounted on the same slide with sections from the corresponding non-implanted half (referred to as “distal” tissue) so that both sections received equal reagent exposure.

Table 1 lists the antibodies used, along with working dilutions and sources. Rod bipolar cells were labeled with anti-protein kinase C alpha subunit (PKCα) (Kosaka et al., 1998). Müller glial reaction in response to ocular stress was assessed with antibodies to glial fibrillary acidic protein (GFAP) (Bringmann et al., 2006). Finally, cholinergic amacrine cells and IPL lamination patterns were visualized with anti-choline acetyltransferase (ChAT) antibodies (Dijk and Kamphuis, 2004). The incubation protocol has been described previously (Lee et al., 2008). Briefly, following a wash in 1.0 M PBS slides were blocked for 1 hour at room temperature (10% donkey serum, 1% BSA, and 1% Triton X-100 in 1.0 M PBS). Primary and secondary antibodies were diluted in 1.0 M PBS containing 0.5% Triton X-100. Sections were incubated with primary antibodies overnight at 4°C and secondary antibodies for 2 hours at room temperature. Fluorescent secondary antibodies included donkey-anti-rabbit-DyLight® 488 (Abcam, Cambridge, MA) and donkey-anti-goat-DyLight® 594 (Abcam, Cambridge, MA), both diluted 1:300. Sections were stained with DAPI, mounted with mounting medium (VectaShield® Hard Set, Vector Laboratories, Inc., Burlingame, CA), and coverslipped.

Sections were visualized and images taken on a confocal microscope (Eclipse Ti microscope with D-Eclipse C1 confocal controller, Nikon, Tokyo). Z-stack images spanning the section thickness at 1 μm intervals were captured using a 40 X oil immersion lens directly under the implant site (“implanted”), immediately adjacent to the implant site (“adjacent”), and “distal” tissue from the non-implanted portion of the eye (see Figure 1A). Images of unimplanted control tissue were acquired from central, superior retinal sections. The Z-stack images were condensed into max-intensity volume projections and processed using commercial software (ImageJ, NIH, Bethesda, MD and Photoshop™6.0, Adobe Systems, Inc., San Jose, CA). For comparisons of cross sections, extended-focus confocal images were composed of a stack of 26 images along the z-axis. ChAT flat mounted extended-focus confocal images were comprised of a stack of 5 planes, each 1 μm thick. Pinhole size, gain, photo multiplier, and

offset of the confocal microscope were standardized within experimental groups. Brightness and contrast optimization was applied equally across all images, except images of GFAP-labeled sections in which no optimization was performed.

2.4.2 Quantification

Digital confocal cross-sections were analyzed using an image program (Image J, National Institute of Health, Bethesda, MA). Cross-sections of immuno-labeled S334ter-3 retinas, implanted with either mPVA or bPVA were quantified in the following ways: 1) the length of PKCα labeled rod bipolar cells were measured from the center of the soma to the axon terminals, 2) intensity of GFAP immunofluorescence was measured, and 3) the number of INL-placed and displaced (in RGC layer) ChAT-positive amacrine nuclei were counted. For each quantification, at least 2 sections from 2-4 retinas were analyzed. Triplicate measurements of rod bipolar cells from summed z-stack PKCα-labeled images were made on each section and averaged. GFAP immunoreactivity was quantified by measuring the intensity of a 55 x 40 μm region of interest (ROI) beginning at the retinal ganglion cell layer extending into the inner plexiform layer and normalized to a background region without tissue of similar size. PKCα and GFAP data was normalized to the distal regions to compare implant designs between different ages. ChAT-labeled z-stacks were summed and the number of ChAT positive nuclei was measured along a 150-μm length on each section.

Statistical comparisons between mPVA and bPVA devices from each retinal region were made with two-way repeated measures ANOVA using Holm-Sidak post-hoc comparisons (Sigmastat v3.5 ,Systat Software, San Jose, CA).

2.4.3 Flat mounts

A subset of RCS eyes was processed as flat mounts, as described previously (Bernstein and Guo, 2011), with the following modifications. Eyes were enucleated and fixed in 4%

paraformaldehyde for 2 hours. The posterior eye cups were digested in hyaluronidase (1mg/mL; Sigma-Aldrich, St. Louis, MO) diluted 1:500 in 1.0 M PBS for 30 minutes. The retinas were carefully dissected from the retinal pigment epithelium (RPE), washed twice in PBST (0.5% Triton X-100 in 1.0M PBS), and then frozen in PBST at -80°C for 15 minutes. After thawing slowly at room temperature, the retina was washed twice in PBST, blocked (10% donkey serum, 0.25% Triton X-100 in 1.0M PBS) for 4 hours at room temperature, and incubated in anti-ChAT antibody (Table 1) overnight at 4°C. After 3 washes in PBST, donkey-anti-goat-DyLight® 594 secondary antibody (1:300; Abcam, Cambridge, MA) was applied for 1 hour at room temperature. Following additional washes, retinas were stained with DAPI, cut into a cloverleaf shape, and flattened on glass slides with the RGC layer face up. The retinas were mounted with mounting medium (VectaShield® Hard Set, Vector Laboratories, Inc., Burlingame, CA) and coverslipped.

The flat mounts were imaged using the confocal system, as described above, to generate Z-stack images over the implant site and distal regions of the same retina. 3D recreations were assembled and rotated using the 3D Viewer Plugin (ImageJ, NIH, Bethesda, MD). Contrast and brightness were optimized equally across images (Photoshop™6.0, Adobe Systems, Inc., San Jose, CA).

3. Results

3.1 Rod bipolar cells maintained in both implant designs and RP models

Rod bipolar cells were labeled for PKCα in both RCS and S334ter-3 rat eyes implanted with either PVA design. Figure 1A shows a fundus image of an mPVA in an RCS rat and the superimposed colored lines indicate the areas of the retina sampled in each of the subsequent figures. Blue indicates the area within the implant site, red the area adjacent to and green the area distal to the implant site.

Figure 1 shows representative images of PKCα positive rod bipolar cells in wild-type (WT) (Figure 1B) and RCS rat retinas. An unimplanted RCS retina is shown in Figure 1F. The unimplanted and the implanted RCS retinas exhibited atrophy of rod bipolar cell dendritic tufts relative to WT. In implanted retinas, this was the case both within and outside implant sites. In all RCS retinas, rod bipolar cells retained the other aspects of their characteristic morphology; their somas were located near the outer margin of the INL and axon terminals in the distal IPL. In addition, they persisted across the retina, including within the implant site regardless of device design (Figure 1C, G). There were no apparent disruptions of rod bipolar cell morphology between implant site, adjacent, and distal sites for both bPVA and mPVA implants (compare Figure 1 C,G to D,H to E,I).

Implantation of subretinal devices in S334ter-3 rats had no effect on rod bipolar cell morphology. Unimplanted S334ter-3 control retinas (Figure 2E) showed a complete loss of rod bipolar cell dendritic arbors, disorganization of their somas, and a considerably thinner INL compared to WT (Figure 2A); demonstrating a more advanced retinal degeneration compared to RCS rats (Figures 1F and 2E). Similarly, S334ter-3 morphology of rod bipolar cells was comparable regardless of PVA design (Figure 2B-D and 2F-H). S334ter- 3 rod bipolar cells retained their characteristic morphology with somas near the outer margin of the INL and axon terminals in the distal IPL. In addition, there was no apparent disruption of rod bipolar cell morphology between implant site, adjacent, and distal sites in the S334ter-3 rat (Figures 2B-D and F-H), regardless of device design. Quantification of the length of PKCα labeled rod bipolar cells in S344ter-3 rats showed no significant differences between mPVA and bPVA implanted rats or retinal location (Figure 3A; Two-way repeated ANOVA, $p>0.05$).

3.2 Cholinergic amacrine cells intact with implantation of PVA devices

RCS and S334ter-3 sections were labeled with ChAT to explore the organization of the cholinergic amacrine cells and the laminar bands that their processes form in the IPL (Figure 4). The pattern of ChAT expression indicated that cholinergic amacrine cells survive within the implant site and both their somas and processes maintain WT IPL lamination patterns, with cell bodies in both the ganglion cell layer (GCL) and the innermost layer of the INL, and stratified processes within sublaminae a and b (Figure 4). RCS and S334ter-3 tissue showed identical expression patterns in unimplanted control, implanted, adjacent, and distal retinal tissue with implantation of the bPVA (Figure 4B-I). mPVA-implanted retinas maintained this typical pattern (data not shown). Counts of ChAT labeled nuclei in S334ter-3 eyes in both the INL and ganglion cell layer had a trend towards being lower in mPVA than bPVA, but did not differ statistically (Figure 3C, 3D; Two-way repeated ANOVA, p=0.111 and p = 0.112, respectively). ChAT expression pattern also was examined *en face* in retinal flat mounts in a subset of RCS rats (Figure 5). The general distribution of ChAT-labeled cells was consistent between control and both mPVA implanted retinas for ChAT-labeled cells in both the INL and ganglion cell, which tiled the retina in a mosaic fashion as expected (Figure 5A vs 5B and 5C vs 5D, respectively).

3.3 Müller cell glial reaction within normal limits after implantation

Glial reaction within RCS and S334ter-3 retina was evaluated using expression of GFAP (Figure 6). RCS age-matched unimplanted retinas (Figure 6A) displayed strong GFAP labeling in Müller glial processes that extended from the nerve fiber layer (NFL) to the partially degenerated ONL. In bPVA implanted RCS retinas at 4 weeks post implantation (Figure 6B-D), the glial reaction within the implant site was similar to the reaction in adjacent and distal regions; we observed little to no additional glial scarring around the implant (Figure 6B). In fact, in many cases, GFAP labeling appeared to be less pronounced at the implant site (Figure 6B) relative to distal areas (Figure 6D). Similar results were found with mPVA devices (data not shown).

S334ter-3 age-matched unimplanted retinas showed intense GFAP labeling at the outer edge of the INL that was not seen in RCS retina (Figure 6A, E, I). This is consistent with the faster degeneration in this model and the formation of a glial seal that occurs after total photoreceptor degeneration (Jones et al., 2003). While glial reaction was widespread, persistent, and uniform in all S334ter-3 tissue, there was no noticeable difference in expression of GFAP by Müller glia in bPVA implanted retinas adjacent or distal to the implants (Figure 6J-L). Although the spatial extent of GFAP reaction was similar in mPVA implanted retinas (Figure 6F-H), we observed a significant increase in GFAP intensity in mPVA devices compared to bPVA (Figure 3B; Two-way repeated ANOVA, main effect of device, $F(1, 15) = 14.38$, $p=0.02$; Figure 3B). The differences were greatest over the implant regions with bPVA-implanted retinas having less GFAP immunoreactivity.

4. Discussion

The use of subretinal prostheses for the restoration of vision in patients with RP or AMD depends upon an intact inner retina (O'Brien et al., 2012). Thus, it is critical that implantation of a subretinal device does not cause a loss of inner retinal cells or excessive gliosis/fibrosis, as both would interfere with the retinal-prosthesis interface. We have shown that a functional connection that requires synaptic transmission within the inner retina drives PVA evoked responses in the superior colliculus (Fransen et al., 2014). Here we show that the morphological basis for this connectivity is an intact inner retina in subretinally-implanted m- and bPVA devices. In addition, we show that morphology is maintained in two RP rat models, one with direct photoreceptor degeneration, the other with RPE dysfunction induced photoreceptor degeneration. This indicates that the effect we observe is general. We assessed rod bipolar cells because they represent the primary transmission pathway from the PVA to the RGCs and cholinergic amacrine cells because they are one of the most numerous amacrine cells and their processes form well known sublaminae in the the IPL. Together the two measures provide a

general assessment of inner retinal cell organization. While it is well-established that the degenerating retina undergoes remodeling when all photoreceptors are lost (Gargini et al., 2007; Marc et al., 2003; Strettoi et al., 2002), we show that in these models, rod bipolar cells and cholinergic amacrine cells within the implant site continue to exhibit typical and well-preserved morphology. Both their somata and processes within the IPL show normal localization and lamination. Previous studies show that normal retinas respond to both acute epiretinal electrical stimulation (Ray et al., 2009; Ray et al., 2011), or chronic subretinal implantation (Chow et al., 2001; Pardue et al., 2001; Tamaki et al., 2008; Yu et al., 2009) with an upregulation of GFAP expression and degenerative changes to the dendrites of rod bipolar cells. One study in which photosensitive dye-coupled film was subretinally implanted into RCS rat eyes showed preservation within the implant site of rod bipolar cell morphology via PKCα labeling (Alamusi et al., 2013), consistent with the findings we report here.

The increase in GFAP labeling in all unimplanted RCS and S334ter-3 retinas compared to WT (images not shown) is consistent with previous reports on retinal remodeling during degeneration (Marc and Jones, 2003; Zhao et al., 2012). Importantly, GFAP labeling in and around the implant site was similar to distal areas, suggesting that the glial reaction was not augmented by the presence of the PVA. Previous immunohistochemical studies of subretinal implants in animals with normal retinas have shown an increase in GFAP expression within the implant site (Chow et al., 2001; Pardue et al., 2001; Tamaki et al., 2008; Yu et al., 2009). It is feasible that any upregulation in GFAP due to implantation is masked when extensive gliosis due to photoreceptor degeneration is already present. Quantification of GFAP immunofluorescence showed a significant decrease in S334ter-3 retinas implanted with bPVAs compared to mPVAs. This may indicate that the gap design of the bPVA is more biocompatible with the retina and reduces the stress response. As the PVA devices are active and present electrical current to the underlying inner retina in response to light, it is possible that GFAP

339 expression in the Müller glia is tempered by neuroprotective effects of subretinal electrical
340 stimulation, which have been characterized previously (Ciavatta et al., 2013; Pardue et al.,
341 2005a; Pardue et al., 2005b).

342 The persistence of inner retinal cells and their intact organization under the implanted
343 device are consistent with our finding that PVA evoked responses are retained in the superior
344 colliculus and require inner retinal synaptic transmission (Fransen et al., 2014). Structural
345 integrity is critical to the success of function using this subretinal approach to visual restoration.
346 The presence of normal IPL sublamination suggests that other circuits that modulate the
347 excitatory signal are retained and may provide even better RGC and central signals. When
348 translated to the clinic, implantation will be performed at mid to late stage of photoreceptor
349 degeneration, similar to the implantation stages used here in the RCS and S334ter-3 rats,
350 respectively. The morphology of the retina implanted with both PVAs was similar, which also is
351 consistent with the functional results (Fransen et al., 2014) suggesting good compatibility at
352 both stages of degeneration.

353 The development of the next-generation bPVA is intended to improve upon the design of
354 the mPVA device, which has already been implanted in human patients (Chow et al., 2010;
355 Chow et al., 2004). Bipolar design of the pixel electrodes provides much tighter confinement of
356 electric field, and appears to improve spatial resolution, compared to monopolar arrangement in
357 mPVAs (Fransen et al., 2014). Our comparisons between mPVA- and bPVA-implanted retinas
358 and the reduced glial reaction in the retinas implanted with the bPVA device with the gaps
359 between pixels suggests improved biocompatibility and may indicate a longer duration of the
360 interface between the device and the retina, which needs to be tested empirically.

361 **5. Conclusions**

We found that both mPVA and bPVA devices implanted into the subretinal space were well tolerated by the inner retina in two rat models of RP with regard to rod bipolar, cholinergic amacrine, and Müller cell morphology. This initial analysis could be complemented with assays of other cell types (such as cone bipolar cells, horizontal cells as well as other amacrine cell classes). Other functional analyses could be aimed at examining the RGC responses and the timing and spatial distribution of their excitatory and inhibitory inputs. With our findings this would provide a complete understanding of the morphological and functional status of the inner retina in contact with the prosthesis.

Acknowledgements

Funding was provided by the National Institutes of Health (R01-EY018608), the Air Force Office of Scientific Research (FA9550-04), NIH CTSA (UL1 RR025744, Stanford Spectrum fund) and a Stanford Bio-X IIP grant. K.M. was supported by an SU2P fellowship as part of an RCUK Science Bridges award. J.F. was supported by an NIH T32 grant (5 T32 HL 76138-09). M.T.P. was supported by a Research Career Scientist Award from the Department of Veterans Affairs.

Table 1: Primary antibodies used in this study to characterize inner retinal health.

Antigen	Antiserum	Source	Working Dilution	Cellular Target
PKCα	Polyclonal rabbit anti-PKCα	Santa Cruz Biotechnology, Inc., Dallas, TX	1:2000	Rod bipolar cells
GFAP	Polyclonal rabbit anti-GFAP	Abcam, Cambridge, MA	1:500	Glial reaction in retinal Müller cells
ChAT	Polyclonal goat anti-ChAT	Millipore, Billerica, MA	1:100	Cholinergic amacrine cells

Figures Captions

Figure 1. A) Sample fundus image of an RCS rat eye implanted subretinally with an mPVA. White dotted line indicates location of the cut made in the superior to inferior plane bisecting the posterior eye cup into implanted and non-implanted halves. “Implanted” region is indicated by the blue line. The area immediately “adjacent” to the implant site is shown by the red line. The green line displays an area opposite the implant within the non-implanted half, referred to as a “distal” area. The implant is 1mm in diameter. PKCα labeling in retinal cross-sections from WT rats (B), unimplanted control RCS rats at 2 months of age (F), RCS rats implanted from 4 to 8 weeks postnatal with a bPVA (C-E) and or mPVA (G-I). Rod bipolar cells are present with well-preserved morphology and localization at the implant site (C and G) relative to adjacent (D and H) and distal (E and I) regions. Implanted eyes show PKCα labeling consistent with that of age-matched unimplanted RCS controls (F). Wild-type retinas (B) appear to exhibit more intact dendritic tufts, but somata and axon terminal localization is comparable to that in RCS tissue. Insets 1B, 1C, 1 F & 1G show magnified images of the dendritic tufts in the OPL. ONL=outer nuclear layer, OPL=outer plexiform layer, INL=inner nuclear layer, IPL=inner plexiform layer, GCL=ganglion cell layer. Scale bar=50μm.

Figure 2. PKCα labeling in retinal cross-sections from S334ter-3 rats implanted with a bPVA (B-D, implanted from 7 to 27 weeks postnatal) or mPVA (F-H, implanted from 6 to 27 weeks postnatal). Implanted sections (B and F) show rod bipolar cell morphology that is comparable to that in adjacent (C and G) and distal (D and H) areas. The morphology and localization of these sections is consistent with that seen in age-matched unimplanted S334ter-3 controls (E). However, all S334ter-3 tissues exhibit virtually complete loss of the ONL and rod bipolar cell dendrites, both of which are still evident in wild-type retina (A). Scale bar=50μm.

Figure 3. PKCα, GFAP, and ChAT labeling quantification. The relative length of PKCα-labeled bipolar cells (A) did not show significant differences between retinal region or implant types. The intensity of GFAP immunoreactivity (B) did not show significant differences between the retinal

location within each implant type, but did show a difference between implant types (Two-way repeated ANOVA, $F(1, 15) = 14.38$ $p = 0.02$, $n = 6$). Immunoreactivity was normalized to the distal position for the PKCα and GFAP labeling. ChAT immunoreactive cell counts did not show significant differences between retinal location or implant type for either INL placed (C) or displaced (D) cholinergic amacrine cells. Error bars represent standard error of the mean.

Figure 4. ChAT labeling in retinal cross-sections from RCS eyes (C-E, implanted from 4 to 8 weeks postnatal) and S334ter-3 eyes (G-I, implanted from 7 to 27 weeks postnatal) with bPVA devices. Both RCS (B-E) and S334ter-3 sections (F-I), like wild-type (A), show typical cholinergic amacrine cell morphology with somata in the INL and GCL and processes in a dual-lamination pattern within the IPL. ChAT labeling patterns in implanted areas (C and G) are identical to those in adjacent (D and H), distal (E and I), Scale bar=50μm.

Figure 5. ChAT-labeled retinal flat mounts from RCS rats implanted from 4 to 8 weeks postnatal with an mPVA device (C and D) compared to unimplanted control eyes (A and B). *En face* view of unimplanted INL placed (A) and implanted INL placed (C) ChAT positive amacrine cells shows similar cholinergic amacrine cell distribution with consistent density. Similarly, labelling patterns of ChAT positive amacrine cells in the ganglion cell layer were consistent between unimplanted (B) and implanted (D) retinas. Scale bar=50μm.

Figure 6. GFAP labeling in retinal cross-sections from RCS (B-D) with bPVA and S334ter-3 eyes with mPVA (F-H) and bPVA (K-L) devices. RCS were implanted 4 to 8 weeks postnatally, while the S334ter-3 animals were implanted at 12 to 32 weeks. Glial reaction is widespread in all RCS tissue (A-D), but implanted areas (B) do not show increased GFAP labeling in comparison with adjacent (C), distal (D), and age-matched unimplanted control (A) sections. Similar to RCS tissue, S334ter-3 sections (E-L) show widespread gliosis due to photoreceptor degeneration. However, GFAP labeling is not augmented in implanted regions (F and J) relative

to adjacent (G and K), distal (H and L), and age-matched unimplanted control section (E). S334ter-3 retinas display a characteristic glial seal above the INL, not seen in wild-type retinas (data not shown), consistent with advanced photoreceptor degeneration. NFL=nerve fiber layer. Scale bar=50μm.

References

Adkins, A., Wang, W., Kaplan, H., Emery, D., Fernandez de Castro, J., Lee, S.-J., Huie, P., Palanker, D., McCall, M., Pardue, M., 2013. Morphological comparisons of flat and 3-dimensional subretinal photovoltaic arrays in rat and pig models of retinitis pigmentosa. Invest. Ophthalmol. Vis. Sci. 54, 1038.

Alamusi, Matsuo, T., Hosoya, O., Tsutsui, K.M., Uchida, T., 2013. Behavior tests and immunohistochemical retinal response analyses in RCS rats with subretinal implantation of Okayama-University-type retinal prosthesis. J. Artif. Organs 16, 343-351.

Asher, A., Segal, W.A., Baccus, S.A., Yaroslavsky, L.P., Palanker, D.V., 2007. Image processing for a high-resolution optoelectronic retinal prosthesis. IEEE Trans. Biomed. Eng. 54, 993-1004.

Bernstein, S.L., Guo, Y., 2011. Changes in cholinergic amacrine cells after rodent anterior ischemic optic neuropathy (rAION). Invest. Ophthalmol. Vis. Sci. 52, 904-910.

Bi, A.D., Cui, J.J., Ma, Y.P., Olshevskaya, E., Pu, M.L., Dizhoor, A.M., Pan, Z.H., 2006. Ectopic expression of a microbial-type rhodopsin restores visual responses in mice with photoreceptor degeneration. Neuron 50, 23-33.

Bringmann, A., Pannicke, T., Grosche, J., Francke, M., Wiedemann, P., Skatchkov, S.N., Osborne, N.N., Reichenbach, A., 2006. Muller cells in the healthy and diseased retina. Prog. Retin. Eye Res. 25, 397-424.

Busskamp, V., Picaud, S., Sahel, J.A., Roska, B., 2012. Optogenetic therapy for retinitis pigmentosa. Gene Ther. 19, 169-175.

Chow, A.Y., Bittner, A.K., Pardue, M.T., 2010. The artificial silicon retina in retinitis pigmentosa patients (an American Ophthalmological Association thesis). Trans. of the Am. Ophthalmol. Soc. 108, 120-154.

480 Chow, A.Y., Chow, V.Y., Packo, K.H., Pollack, J.S., Peyman, G.A., Schuchard, R., 2004. The
481 artificial silicon retina microchip for the treatment of vision loss from retinitis pigmentosa.
482 Arch. Ophthalmol. 122, 460-469.
483 Chow, A.Y., Pardue, M.T., Chow, V.Y., Peyman, G.A., Liang, C., Perlman, J.I., Peachey, N.S.,
484 2001. Implantation of silicon chip microphotodiode arrays into the cat subretinal space.
485 IEEE Trans. Neural Syst. Rehabil. Eng. 9, 86-95.
486 Ciavatta, V.T., Mocko, J.A., Kim, M.K., Pardue, M.T., 2013. Subretinal electrical stimulation
487 preserves inner retinal function in RCS rat retina. Mol. Vis. 19, 995-1005.
488 Cicione, R., Shivdasani, M.N., Fallon, J.B., Luu, C.D., Allen, P.J., Rathbone, G.D., Shepherd,
489 R.K., Williams, C.E., 2012. Visual cortex responses to suprachoroidal electrical
490 stimulation of the retina: effects of electrode return configuration. J. Neural Eng. 9,
491 036009.
492 Dijk, F., Kamphuis, W., 2004. An immunocytochemical study on specific amacrine cell
493 subpopulations in the rat retina after ischemia. Brain Res. 1026, 205-217.
494 Fransen, J. W., Pangeni, G., Pardue, M.T., McCall, M.A. 2014. Local signaling from a retinal
495 prosthetic in a rodent retinitis pigmentosa model in vivo. J. Neural Eng. 11, 046012.
496 Garg, S.J., Federman, J., 2013. Optogenetics, visual prosthesis and electrostimulation for
497 retinal dystrophies. Curr. Opin. Ophthalmol. 24, 407-414.
498 Gargini, C., Terzibasi, E., Mazzoni, F., Strettoi, E., 2007. Retinal organization in the retinal
499 degeneration 10 (rd10) mutant mouse: a morphological and ERG study. J. Comp.
500 Neurol. 500, 222-238.
501 Grünert, U., Martin ,P.R.,1991. Rod bipolar cells in the macaque monkey retina:
502 immunoreactivity and connectivity. J Neurosci. 11, 2742-2758.
503 Hartong, D.T., Berson, E.L., Dryja, T.P., 2006. Retinitis pigmentosa. Lancet 368, 1795-1809.
504 Humayun, M.S., Dorn, J.D., da Cruz, L., Dagnelie, G., Sahel, J.A., Stanga, P.E., Cideciyan,
505 A.V., Duncan, J.L., Eliott, D., Filley, E., Ho, A.C., Santos, A., Safran, A.B., Arditi, A., Del

506 Priore, L.V., Greenberg, R.J., Argus, I.I.S.G., 2012. Interim results from the international
507 trial of Second Sight's visual prosthesis. Ophthalmology 119, 779-788.
508 Humayun, M.S., Prince, M., de Juan, E., Barron, Y., Moskowitz, M., Klock, I.B., Milam, A.H.,
509 1999. Morphometric analysis of the extramacular retina from postmortem eyes with
510 retinitis pigmentosa. Invest. Ophthalmol. Vis. Sci. 40, 143-148.
511 Isago, H., Sugano, E., Wang, Z., Murayama, N., Koyanagi, E., Tamai, M., Tomita, H., 2012.
512 Age-Dependent Differences in Recovered Visual Responses in Royal College of
513 Surgeons Rats Transduced with the Channelrhodopsin-2 Gene. J. of Mol. Neurosci. 46,
514 393-400.
515 Jensen, R.J., Ziv, O.R., Rizzo, J.F., 2005. Responses of rabbit retinal ganglion cells to electrical
516 stimulation with an epiretinal electrode. J. Neural Eng. 2, S16-21.
517 Jones, B.W., Watt, C.B., Frederick, J.M., Baehr, W., Chen, C.K., Levine, E.M., Milam, A.H.,
518 Lavail, M.M., Marc, R.E., 2003. Retinal remodeling triggered by photoreceptor
519 degenerations. J. Comp. Neurol. 464, 1-16.
520 Jones, B.W., Marc, R.E., 2005. Retinal remodeling during retinal degeneration. Exp. Eye Res.
521 81, 123-137.
522 Kanda, H., Morimoto, T., Fujikado, T., Tano, Y., Fukuda, Y., Sawai, H., 2004.
523 Electrophysiological studies of the feasibility of suprachoroidal-transretinal stimulation for
524 artificial vision in normal and RCS rats. Invest. Ophthalmol. Vis. Sci. 45, 560-566.
525 Kosaka, J., Suzuki, A., Morii, E., Nomura, S., 1998. Differential localization and expression of
526 alpha and beta isoenzymes of protein kinase C in the rat retina. J. Neurosci. Res. 54,
527 655-663.
528 LaVail, M.M., Battelle, B.A., 1975. Influence of eye pigmentation and light deprivation on
529 inherited retinal dystrophy in the rat. Exp. Eye Res. 21, 167-192.
530 LaVail, M.M., Sidman, R.L., Gerhardt, C.O., 1975. Congenic strains of RCS rats with inherited
531 retinal dystrophy. J. Hered. 66, 242-244.

532 Lee, E.J., Padilla, M., Merwine, D.K., Grzywacz, N.M., 2008. Developmental regulation of the
533 morphology of mouse retinal horizontal cells by visual experience. Eur. J. Neurosci. 27,
534 1423-1431.
535 Lin, B., Koizumi, A., Tanaka, N., Panda, S., Masland, R.H., 2008. Restoration of visual function
536 in retinal degeneration mice by ectopic expression of melanopsin. Proc. Natl. Acad. Sci.
537 U.S.A. 105, 16009-16014.
538 Mandel, Y., Goetz, G., Lavinsky, D., Huie, P., Mathieson, K., Wang, L., Kamins, T., Galambos,
539 L., Manivanh, R., Harris, J., Palanker, D., 2013. Cortical responses elicited by
540 photovoltaic subretinal prostheses exhibit similarities to visually evoked potentials. Nat.
541 Commun. 4, 1980.
542 Marc, R.E., Jones, B.W., 2003. Retinal remodeling in inherited photoreceptor degenerations.
543 Mol. Neurobiol. 28, 139-147.
544 Marc, R.E., Jones, B.W., Anderson, J.R., Kinard, K., Marshak, D.W., Wilson, J.H., Wensel, T.,
545 Lucas, R.J., 2007. Neural reprogramming in retinal degeneration. Invest. Ophthalmol.
546 Vis. Sci. 48, 3364-3371.
547 Marc, R.E., Jones, B.W., Watt, C.B., Strettoi, E., 2003. Neural remodeling in retinal
548 degeneration. Prog. Retin. Eye Res. 22, 607-655.
549 Mathieson, K., Loudin, J., Goetz, G., Huie, P., Wang, L., Kamins, T.I., Galambos, L., Smith, R.,
550 Harris, J.S., Sher, A., Palanker, D., 2012. Photovoltaic Retinal Prosthesis with High Pixel
551 Density. Nat. Photonics 6, 391-397.
552 McGill, T.J., Prusky, G.T., Douglas, R.M., Yasumura, D., Matthes, M.T., Lowe, R.J., Duncan,
553 J.L., Yang, H., Ahern, K., Daniello, K.M., Silver, B., LaVail, M.M., 2012. Discordant
554 anatomical, electrophysiological, and visual behavioral profiles of retinal degeneration in
555 rat models of retinal degenerative disease. Invest. Ophthalmol. Vis. Sci. 53, 6232-6244.
556 Morimoto, T., Kamei, M., Nishida, K., Sakaguchi, H., Kanda, H., Ikuno, Y., Kishima, H., Maruo,
557 T., Konoma, K., Ozawa, M., Nishida, K., Fujikado, T., 2011. Chronic Implantation of

Newly Developed Suprachoroidal-Transretinal Stimulation Prosthesis in Dogs. Invest. Ophthalmol. Vis. Sci. 52, 6785-6792.

Mullen, R.J., LaVail, M.M., 1976. Inherited retinal dystrophy: primary defect in pigment epithelium determined with experimental rat chimeras. Science 192, 799-801.

O'Brien, E.E., Greferath, U., Vessey, K.A., Jobling, A.I., Fletcher, E.L., 2012. Electronic restoration of vision in those with photoreceptor degenerations. Clin. Exp. Optom. 95, 473-483.

Palanker, D., Huie, P., Vankov, A., Aramant, R., Seiler, M., Fishman, H., Marmor, M., Blumenkranz, M., 2004. Migration of retinal cells through a perforated membrane: implications for a high-resolution prosthesis. Invest. Ophthalmol. Vis. Sci. 45, 3266-3270.

Pardue, M.T., Phillips, M.J., Yin, H., Fernandes, A., Cheng, Y., Chow, A.Y., Ball, S.L., 2005a. Possible sources of neuroprotection following subretinal silicon chip implantation in RCS rats. J. Neural Eng. 2, S39-47.

Pardue, M.T., Phillips, M.J., Yin, H., Sippy, B.D., Webb-Wood, S., Chow, A.Y., Ball, S.L., 2005b. Neuroprotective effect of subretinal implants in the RCS rat. Invest. Ophthalmol. Vis. Sci. 46, 674-682.

Pardue, M.T., Stubbs, E.B., Jr., Perlman, J.I., Narfstrom, K., Chow, A.Y., Peachey, N.S., 2001. Immunohistochemical studies of the retina following long-term implantation with subretinal microphotodiode arrays. Exp. Eye Res. 73, 333-343.

Ray, A., Colodetti, L., Weiland, J.D., Hinton, D.R., Humayun, M.S., Lee, E.J., 2009. Immunocytochemical analysis of retinal neurons under electrical stimulation. Brain Res. 1255, 89-97.

Ray, A., Lee, E.J., Humayun, M.S., Weiland, J.D., 2011. Continuous electrical stimulation decreases retinal excitability but does not alter retinal morphology. J. Neural Eng. 8, 045003.

583 Rizzo, J.F., 3rd, 2011. Update on retinal prosthetic research: the Boston Retinal Implant Project.
584 J. Neuroophthalmol. 31, 160-168.
585 Strettoi, E., Porciatti, V., Falsini, B., Pignatelli, V., Rossi, C., 2002. Morphological and functional
586 abnormalities in the inner retina of the rd/rd mouse. J. Neurosci. 22, 5492-5504.
587 Strettoi, E., Pignatelli, V., Rossi, C., Porciatti, V., Falsini, B., 2003. Remodeling of second-order
588 neurons in the retina of rd/rd mutant mice. Vision Research 43, 867–877.

589 Tamaki, T., Matsuo, T., Hosoya, O., Tsutsui, K.M., Uchida, T., Okamoto, K., Uji, A., Ohtsuki, H.,
590 2008. Glial reaction to photoelectric dye-based retinal prostheses implanted in the
591 subretinal space of rats. J. Artif. Organs 11, 38-44.
592 Tomita, H., Sugano, E., Yawo, H., Ishizuka, T., Isago, H., Narikawa, S., Kugler, S., Tamai, M.,
593 2007. Restoration of visual response in aged dystrophic RCS rats using AAV-mediated
594 channelopsin-2 gene transfer. Invest. Ophthalmol. Vis. Sci. 48, 3821-3826.
595 Uji, A., Matsuo, T., Ishimaru, S., Kajiura, A., Shimamura, K., Ohtsuki, H., Dan-oh, Y., Suga, S.,
596 2005. Photoelectric dye-coupled polyethylene film as a prototype of retinal prostheses.
597 Artif. Organs 29, 53-57.
598 Wang, L., Mathieson, K., Kamins, T.I., Loudin, J.D., Galambos, L., Goetz, G., Sher, A., Mandel,
599 Y., Huie, P., Lavinsky, D., Harris, J.S., Palanker, D.V., 2012. Photovoltaic retinal
600 prosthesis: implant fabrication and performance. J. Neural Eng. 9, 046014.
601 Wong, Y.T., Chen, S.C., Seo, J.M., Morley, J.W., Lovell, N.H., Suaning, G.J., 2009. Focal
602 activation of the feline retina via a suprachoroidal electrode array. Vis. Res. 49, 825-833.
603 Yamauchi, Y., Franco, L.M., Jackson, D.J., Naber, J.F., Ziv, R.O., Rizzo, J.F., Kaplan, H.J.,
604 Enzmann, V., 2005. Comparison of electrically evoked cortical potential thresholds
605 generated with subretinal or suprachoroidal placement of a microelectrode array in the
606 rabbit. J. Neural Eng. 2, S48-56.

Yu, W., Wang, X., Zhao, C., Yang, Z., Dai, R., Dong, F., 2009. Biocompatibility of subretinal parylene-based Ti/Pt microelectrode array in rabbit for further artificial vision studies. J. Ocul. Biol. Dis. Infor. 2, 33-36.

Zhao, T., Li, Y., Weng, C., Yin, Z., 2012. The changes of potassium currents in RCS rat Muller cell during retinal degeneration. Brain Res. 1427, 78-87.

Zrenner, E., Stett, A., Weiss, S., Aramant, R.B., Guenther, E., Kohler, K., Miliczek, K.D., Seiler, M.J., Haemmerle, H., 1999. Can subretinal microphotodiodes successfully replace degenerated photoreceptors? Vis. Res. 39, 2555-2567.

Inner retinal preservation in rat models of retinal degeneration implanted with subretinal photovoltaic arrays

Jacob G. Light[a,b], James W. Fransen[c], Adewumi N. Adekunle[a], Alice Adkins[b], Gobinda Pangeni[d], James Loudin[e], Keith Mathieson[e,g], Daniel V. Palanker[e,f], Maureen A. McCall[c,d], Machelle T. Pardue[a,b].

[a]Ophthalmology, Emory University; [b]Rehab R&D Center of Excellence, Atlanta VA Medical Center; [c]Anatomical Sciences & Neurobiology, [d]Ophthalmology & Visual Sciences, University of Louisville; [e]Hansen Experimental Physics Laboratory, [f]Ophthalmology, Stanford University; [g]Institute of Photonics, University of Strathclyde, UK

Corresponding Author:

Machelle T. Pardue, PhD
Research Service (151Oph)
Atlanta VA Medical Center
1670 Clairmont Rd
Decatur, GA 30033

Ph: 404-321-6111 x7342
Fax: 404-728-4847
mpardue@emory.edu

Abstract:

Photovoltaic arrays (PVA) implanted into the subretinal space of patients with retinitis pigmentosa (RP) are designed to electrically stimulate the remaining inner retinal circuitry in response to incident light, thereby recreating a visual signal when photoreceptor function declines or is lost. Preservation of inner retinal circuitry is critical to the fidelity of this transmitted signal to ganglion cells and beyond to higher visual targets. Post-implantation loss of retinal interneurons or excessive glial scarring could diminish and/or eliminate PVA-evoked signal transmission. As such, assessing the morphology of the inner retina in RP animal models with subretinal PVAs is an important step in defining biocompatibility and predicting success of signal transmission. In this study, we used immunohistochemical methods to qualitatively and quantitatively compare inner retinal morphology after the implantation of a PVA in two RP models: the Royal College of Surgeons (RCS) or transgenic S334ter-line 3 (S334ter-3) rhodopsin mutant rat. Two PVA designs were compared. In the RCS rat, we implanted devices in the subretinal space at 4 weeks of age and histologically examined them at 8 weeks of age and found inner retinal morphology preservation with both PVA devices. In the S334ter-3 rat, we implanted devices at 6 to 12 weeks of age and again, inner retinal morphology was generally preserved with either PVA design 16 to 26 weeks post implantation. Specifically, the length of rod bipolar cells and numbers of cholinergic amacrine cells were maintained along with their characteristic inner plexiform lamination patterns. Throughout the implanted retinas we found nonspecific glial reaction, but none showed additional glial scarring at the implant site. Our results indicate that subretinally implanted PVAs are well-tolerated in rodent RP models and that the inner retinal circuitry is preserved, consistent with our published results showing implant-evoked signal transmission.

Keywords: retina, prosthetic, bipolar cells, amacrine cells, Müller glial cells

1. Introduction

Retinitis pigmentosa (RP) and age-related macular degeneration (AMD) are leading causes of irreversible blindness worldwide (Hartong et al., 2006). In these diseases, vision loss, regardless of underlying etiology, results from degeneration of retinal photoreceptors. Remodeling of the inner retina occurs in late stages of disease (Jones and Marc, 2005; Marc and Jones, 2003; Marc et al., 2007; Strettoi et al., 2002), but photoreceptor degeneration leaves the neurons and circuitry of the inner retina relatively intact for extended periods of time (Humayun et al., 1999; Jones et al., 2003; Marc and Jones, 2003; Marc et al., 2007; Strettoi et al., 2002; Strettoi et al., 2003).

One promising approach that targets the remaining retinal circuitry to restore lost vision uses prosthetic devices to functionally replace photoreceptors. Several different designs and placement strategies are currently being evaluated. Epiretinal placement and stimulation of the retinal ganglion cells (RGC) should require algorithms to selectively achieve information transmission (Jensen et al., 2005; Humayun et al., 2012). Suprachoroidal implants (Cicione et al., 2012; Kanda et al., 2004; Morimoto et al., 2011; Wong et al., 2009; Yamauchi et al., 2005) and subretinal microphotodiode arrays (Chow et al., 2001; Mathieson et al., 2012; Rizzo, 2011; Zrenner et al., 1999) are designed to directly stimulate bipolar cells and theoretically utilize network-mediated retinal stimulation, preserving the integrative properties of second order neurons in the inner plexiform layer (IPL) (Asher et al., 2007; Wang et al., 2012). Other strategies utilize optogenetics to confer light sensitivity to bipolar or RGCs (Bi et al., 2006; Busskamp et al., 2012; Garg and Federman, 2013; Isago et al., 2012; Lin et al., 2008; Tomita et al., 2007) to directly stimulate retinal tissues.

Subretinally placed photovoltaic arrays (PVAs) provide targeted stimulation to the inner nuclear layer (INL) (Fransen et al., 2014) due to their current density distribution and size

(Mathieson et al. 2012). Because bipolar cells are interneurons that connect photoreceptors to RGCs they are involved in signal transmission with PVAs. Retention of these cells and formation of a functional retinal-prosthetic interface would aid in visual restoration. For this to occur there must be a high level of biocompatibility between the retina and prosthesis. As such, measures of the integrity of the bipolar cells and other retinal constituents are critical components to the evaluation of the success of any subretinal prosthetic.

Previous studies have attempted to characterize the condition of implanted and/or electrically stimulated retinal tissue histologically and immunohistochemically (Alamusi et al., 2013; Chow et al., 2001; Pardue et al., 2001; Ray et al., 2009; Ray et al., 2011; Tamaki et al., 2008). However, many of these studies have examined the effects only of certain aspects of the treatment paradigm, such as acute electrical stimulation or biocompatibility of a prosthetic device in wild-type animals that do not exhibit degenerative pathology. In this study, we examined retinal morphology after implantation of two generations of subretinal silicon devices in two RP rat models. We compared a monopolar PVA (mPVA) with no perforations (Chow et al., 2001) to a bipolar PVA (bPVA), which includes bipolar pixels separated by 5 μm gaps (Mathieson et al., 2012). Photovoltaic pixels in monopolar devices have individual active electrodes, but share a common large return electrode on the back side of the implant. Bipolar pixels are composed of 3 photodiodes in series, connected between the active electrode in the center of the pixel and a return electrode surrounding each pixel (Mathieson et al., 2012). All devices in the present study were photoactive. The bPVA gaps enhance proximity of the electrodes to inner retinal neurons and allow diffusion of extracellular milieu through the implant (Adkins et al., 2013; Mathieson et al., 2012). Since the subretinal PVA stimulates retinal neurons that are within close proximity to the electrode (Fransen et al., 2014), we focused our analysis on inner retinal cells that are likely activated by the PVA device. Rod bipolar cells and cholinergic amacrine cells represent well defined populations of cells with robust cellular

markers to assess overall inner retinal health. We also assessed glial reaction in tissues within and distal to the implant site from 16 to 26 weeks post implantation in the S334ter-3 and 4 weeks post implantation in the RCS rat. Our results suggest that both the mPVA and bPVA designs are well tolerated and preserve the necessary inner retinal circuitry that underlie the transmission of signals to the RGCs and beyond (Fransen et al., 2014).

2. Methods

2.1 Animals and Experimental Groups

All animal procedures were approved by the Institutional Animal Care and Use Committee and conformed to the ARVO Statement for the Use of Animals in Ophthalmology and Vision Research. Two models of RP were used: the Royal College of Surgeons (RCS) and S334ter-3 rats from an in-house breeding colony originated from breeders donated by Dr. Matthew LaVail (University of California, San Francisco) (LaVail et al., 1975; Mullen and LaVail, 1976).

The RCS rats (n=4) were implanted binocularly at 4 weeks of age and terminated 4 weeks post-implantation. RCS rats exhibit a moderate rate of photoreceptor degeneration; approximately 50% of the initial ONL thickness was present at the age of implantation (LaVail and Battelle, 1975). Four eyes were implanted with an mPVA device and 4 with a bPVA device. The eyes were divided such that all bPVA-implanted eyes were processed as frozen sections for retinal cross-sections and half the mPVA eyes processed similarly with the remaining prepared as retinal flat mounts.

S334ter-3 rats were implanted monocularly (right eye) with either an mPVA (n=4) or a bPVA (n=7) from 6 to 12 weeks of age and were terminated at 22 to 32 weeks of age (16-26 weeks of implantation). Monocular implantation accommodated superior colliculus recordings that are reported elsewhere (Fransen et al., 2014). The S334ter-3 is a rapid degeneration model

and most photoreceptors had degenerated at the time of implantation (McGill et al., 2012). All S334ter-3 eyes were processed as frozen sections. Additional cross sections were analyzed from three age-matched unimplanted control eyes from each RP strain, as well as 3 eyes from 8-week-old Long Evans wild-type rats acquired from Charles River.

2.2 Overview of Devices

Two types of PVA were explored: mPVA and bPVA (Mathieson et al., 2012; Pardue et al., 2005b). mPVA devices, provided by Optobionics, Inc (Glen Ellyn, IL), were fabricated using previously described thin-film fabrication methods (Chow et al., 2001). The mPVA is a 1 mm diameter silicon disk, 25 μm thick, containing 1200 microphotodiodes with active electrodes on one face and a common return electrode on the back, both coated with iridium oxide (Chow et al., 2001). The bPVA device's photovoltaic arrays were composed of triple-diode pixels fabricated on a silicon wafer. Each pixel contains an active electrode in its center and a return electrode at the circumference. Upon illumination with a pulse of light, each pixel generates a bi-phasic pulse of electric current flowing through the tissue between electrodes, primarily stimulating the inner nuclear layer (INL) cells (Fransen et al., 2014). Electrodes were coated in iridium oxide and the details of manufacturing methods of the bPVA were published previously (Wang et al., 2012). Five-μm wide gaps were etched between adjacent pixels for electrical isolation and to improve nutrients flow through the implant (Mathieson, et al. 2012). The bPVA device measured 0.8 x 1.2 mm and was 30-μm thick. bPVA devices were left in retinal tissue for histological analysis due to tissue destruction caused by removal.

2.3 Surgical Procedure

The surgical methods employed for implantation of the PVAs into the subretinal space have been described previously (Pardue et al., 2005b). Briefly, rats were anesthetized

[ketamine (60 mg/kg) and xylazine (7.5 mg/kg)] and placed into a sterile field. A traction suture was made at the superior limbus and the eye was rotated inferiorly. A ~1.0 mm incision was made in the superior globe reaching the vitreous. The eye was hydrated with a drop of saline, and a 10 minute waiting period was observed which allowed the retina to detach from the RPE. The PVA was then slid into the subretinal space with the electrodes in contact with the retina. Successful subretinal placement was confirmed via fundus examination and subsequent spectral domain-ocular coherence tomography (SD-OCT) imaging (Heidelberg HRA+OCT, Carlsbad, CA) (Fransen et al., 2014). Implants rested in the superior-temporal retina from 0.5 to 1 mm from the optic nerve head.

2.4 Immunohistochemistry

2.4.1 Cross-sections

Following anesthesia [ketamine (60 mg/kg)/xylazine (7.5 mg/kg)] and sacrifice [390 mg/mL pentobarbital sodium (Euthasol, Virbac AH, Inc., Fort Worth, TX)], eyes were immediately enucleated and fixed in 4% paraformaldehyde for 30 minutes. The posterior eyecup was bisected in the superior/inferior plane near the optic nerve, ensuring that the entire implant was intact and present in only one of the two resulting halves (Figure 1A). mPVA devices were gently extracted from the subretinal space using hydrodissection. bPVAs, which contain gaps through which the retinal tissue migrates (Palanker et al., 2004), were left in place to preserve retinal morphology around the implant. The tissue was cryoprotected overnight in 30% sucrose in 0.1M PBS and frozen in embedding medium (O.C.T. Tissue-Tek®, Sakura Finetek, Tokyo). Retinal sections in the superior/inferior plane (20-30 μm) were cut on a cryostat and thaw-mounted on glass slides. Sections containing the implant site were mounted on the same slide with sections from the corresponding non-implanted half (referred to as “distal” tissue) so that both sections received equal reagent exposure.

Table 1 lists the antibodies used, along with working dilutions and sources. Rod bipolar cells were labeled with anti-protein kinase C alpha subunit (PKCα) (Kosaka et al., 1998). Müller glial reaction in response to ocular stress was assessed with antibodies to glial fibrillary acidic protein (GFAP) (Bringmann et al., 2006). Finally, cholinergic amacrine cells and IPL lamination patterns were visualized with anti-choline acetyltransferase (ChAT) antibodies (Dijk and Kamphuis, 2004). The incubation protocol has been described previously (Lee et al., 2008). Briefly, following a wash in 1.0 M PBS slides were blocked for 1 hour at room temperature (10% donkey serum, 1% BSA, and 1% Triton X-100 in 1.0 M PBS). Primary and secondary antibodies were diluted in 1.0 M PBS containing 0.5% Triton X-100. Sections were incubated with primary antibodies overnight at 4°C and secondary antibodies for 2 hours at room temperature. Fluorescent secondary antibodies included donkey-anti-rabbit-DyLight® 488 (Abcam, Cambridge, MA) and donkey-anti-goat-DyLight® 594 (Abcam, Cambridge, MA), both diluted 1:300. Sections were stained with DAPI, mounted with mounting medium (VectaShield® Hard Set, Vector Laboratories, Inc., Burlingame, CA), and coverslipped.

Sections were visualized and images taken on a confocal microscope (Eclipse Ti microscope with D-Eclipse C1 confocal controller, Nikon, Tokyo). Z-stack images spanning the section thickness at 1 μm intervals were captured using a 40 X oil immersion lens directly under the implant site (“implanted”), immediately adjacent to the implant site (“adjacent”), and “distal” tissue from the non-implanted portion of the eye (see Figure 1A). Images of unimplanted control tissue were acquired from central, superior retinal sections. The Z-stack images were condensed into max-intensity volume projections and processed using commercial software (ImageJ, NIH, Bethesda, MD and Photoshop™6.0, Adobe Systems, Inc., San Jose, CA). For comparisons of cross sections, extended-focus confocal images were composed of a stack of 26 images along the z-axis. ChAT flat mounted extended-focus confocal images were comprised of a stack of 5 planes, each 1 μm thick. Pinhole size, gain, photo multiplier, and

offset of the confocal microscope were standardized within experimental groups. Brightness and contrast optimization was applied equally across all images, except images of GFAP-labeled sections in which no optimization was performed.

2.4.2 Quantification

Digital confocal cross-sections were analyzed using an image program (Image J, National Institute of Health, Bethesda, MA). Cross-sections of immuno-labeled S334ter-3 retinas, implanted with either mPVA or bPVA were quantified in the following ways: 1) the length of PKCα labeled rod bipolar cells were measured from the center of the soma to the axon terminals, 2) intensity of GFAP immunofluorescence was measured, and 3) the number of INL-placed and displaced (in RGC layer) ChAT-positive amacrine nuclei were counted. For each quantification, at least 2 sections from 2-4 retinas were analyzed. Triplicate measurements of rod bipolar cells from summed z-stack PKCα-labeled images were made on each section and averaged. GFAP immunoreactivity was quantified by measuring the intensity of a 55 x 40 μm region of interest (ROI) beginning at the retinal ganglion cell layer extending into the inner plexiform layer and normalized to a background region without tissue of similar size. PKCα and GFAP data was normalized to the distal regions to compare implant designs between different ages. ChAT-labeled z-stacks were summed and the number of ChAT positive nuclei was measured along a 150-μm length on each section.

Statistical comparisons between mPVA and bPVA devices from each retinal region were made with two-way repeated measures ANOVA using Holm-Sidak post-hoc comparisons (Sigmastat v3.5 ,Systat Software, San Jose, CA).

2.4.3 Flat mounts

A subset of RCS eyes was processed as flat mounts, as described previously (Bernstein and Guo, 2011), with the following modifications. Eyes were enucleated and fixed in 4%

paraformaldehyde for 2 hours. The posterior eye cups were digested in hyaluronidase (1mg/mL; Sigma-Aldrich, St. Louis, MO) diluted 1:500 in 1.0 M PBS for 30 minutes. The retinas were carefully dissected from the retinal pigment epithelium (RPE), washed twice in PBST (0.5% Triton X-100 in 1.0M PBS), and then frozen in PBST at -80°C for 15 minutes. After thawing slowly at room temperature, the retina was washed twice in PBST, blocked (10% donkey serum, 0.25% Triton X-100 in 1.0M PBS) for 4 hours at room temperature, and incubated in anti-ChAT antibody (Table 1) overnight at 4°C. After 3 washes in PBST, donkey-anti-goat-DyLight® 594 secondary antibody (1:300; Abcam, Cambridge, MA) was applied for 1 hour at room temperature. Following additional washes, retinas were stained with DAPI, cut into a cloverleaf shape, and flattened on glass slides with the RGC layer face up. The retinas were mounted with mounting medium (VectaShield® Hard Set, Vector Laboratories, Inc., Burlingame, CA) and coverslipped.

The flat mounts were imaged using the confocal system, as described above, to generate Z-stack images over the implant site and distal regions of the same retina. 3D recreations were assembled and rotated using the 3D Viewer Plugin (ImageJ, NIH, Bethesda, MD). Contrast and brightness were optimized equally across images (Photoshop™6.0, Adobe Systems, Inc., San Jose, CA).

3. Results

3.1 Rod bipolar cells maintained in both implant designs and RP models

Rod bipolar cells were labeled for PKCα in both RCS and S334ter-3 rat eyes implanted with either PVA design. Figure 1A shows a fundus image of an mPVA in an RCS rat and the superimposed colored lines indicate the areas of the retina sampled in each of the subsequent figures. Blue indicates the area within the implant site, red the area adjacent to and green the area distal to the implant site.

Figure 1 shows representative images of PKCα positive rod bipolar cells in wild-type (WT) (Figure 1B) and RCS rat retinas. An unimplanted RCS retina is shown in Figure 1F. The unimplanted and the implanted RCS retinas exhibited atrophy of rod bipolar cell dendritic tufts relative to WT. In implanted retinas, this was the case both within and outside implant sites. In all RCS retinas, rod bipolar cells retained the other aspects of their characteristic morphology; their somas were located near the outer margin of the INL and axon terminals in the distal IPL. In addition, they persisted across the retina, including within the implant site regardless of device design (Figure 1C, G). There were no apparent disruptions of rod bipolar cell morphology between implant site, adjacent, and distal sites for both bPVA and mPVA implants (compare Figure 1 C,G to D,H to E,I).

Implantation of subretinal devices in S334ter-3 rats had no effect on rod bipolar cell morphology. Unimplanted S334ter-3 control retinas (Figure 2E) showed a complete loss of rod bipolar cell dendritic arbors, disorganization of their somas, and a considerably thinner INL compared to WT (Figure 2A); demonstrating a more advanced retinal degeneration compared to RCS rats (Figures 1F and 2E). Similarly, S334ter-3 morphology of rod bipolar cells was comparable regardless of PVA design (Figure 2B-D and 2F-H). S334ter- 3 rod bipolar cells retained their characteristic morphology with somas near the outer margin of the INL and axon terminals in the distal IPL. In addition, there was no apparent disruption of rod bipolar cell morphology between implant site, adjacent, and distal sites in the S334ter-3 rat (Figures 2B-D and F-H), regardless of device design. Quantification of the length of PKCα labeled rod bipolar cells in S344ter-3 rats showed no significant differences between mPVA and bPVA implanted rats or retinal location (Figure 3A; Two-way repeated ANOVA, $p>0.05$).

3.2 Cholinergic amacrine cells intact with implantation of PVA devices

RCS and S334ter-3 sections were labeled with ChAT to explore the organization of the cholinergic amacrine cells and the laminar bands that their processes form in the IPL (Figure 4). The pattern of ChAT expression indicated that cholinergic amacrine cells survive within the implant site and both their somas and processes maintain WT IPL lamination patterns, with cell bodies in both the ganglion cell layer (GCL) and the innermost layer of the INL, and stratified processes within sublaminae a and b (Figure 4). RCS and S334ter-3 tissue showed identical expression patterns in unimplanted control, implanted, adjacent, and distal retinal tissue with implantation of the bPVA (Figure 4B-I). mPVA-implanted retinas maintained this typical pattern (data not shown). Counts of ChAT labeled nuclei in S334ter-3 eyes in both the INL and ganglion cell layer had a trend towards being lower in mPVA than bPVA, but did not differ statistically (Figure 3C, 3D; Two-way repeated ANOVA, p=0.111 and p = 0.112, respectively). ChAT expression pattern also was examined *en face* in retinal flat mounts in a subset of RCS rats (Figure 5). The general distribution of ChAT-labeled cells was consistent between control and both mPVA implanted retinas for ChAT-labeled cells in both the INL and ganglion cell, which tiled the retina in a mosaic fashion as expected (Figure 5A vs 5B and 5C vs 5D, respectively).

3.3 Müller cell glial reaction within normal limits after implantation

Glial reaction within RCS and S334ter-3 retina was evaluated using expression of GFAP (Figure 6). RCS age-matched unimplanted retinas (Figure 6A) displayed strong GFAP labeling in Müller glial processes that extended from the nerve fiber layer (NFL) to the partially degenerated ONL. In bPVA implanted RCS retinas at 4 weeks post implantation (Figure 6B-D), the glial reaction within the implant site was similar to the reaction in adjacent and distal regions; we observed little to no additional glial scarring around the implant (Figure 6B). In fact, in many cases, GFAP labeling appeared to be less pronounced at the implant site (Figure 6B) relative to distal areas (Figure 6D). Similar results were found with mPVA devices (data not shown).

S334ter-3 age-matched unimplanted retinas showed intense GFAP labeling at the outer edge of the INL that was not seen in RCS retina (Figure 6A, E, I). This is consistent with the faster degeneration in this model and the formation of a glial seal that occurs after total photoreceptor degeneration (Jones et al., 2003). While glial reaction was widespread, persistent, and uniform in all S334ter-3 tissue, there was no noticeable difference in expression of GFAP by Müller glia in bPVA implanted retinas adjacent or distal to the implants (Figure 6J-L). Although the spatial extent of GFAP reaction was similar in mPVA implanted retinas (Figure 6F-H), we observed a significant increase in GFAP intensity in mPVA devices compared to bPVA (Figure 3B; Two-way repeated ANOVA, main effect of device, $F(1, 15) = 14.38$, $p=0.02$; Figure 3B). The differences were greatest over the implant regions with bPVA-implanted retinas having less GFAP immunoreactivity.

4. Discussion

The use of subretinal prostheses for the restoration of vision in patients with RP or AMD depends upon an intact inner retina (O'Brien et al., 2012). Thus, it is critical that implantation of a subretinal device does not cause a loss of inner retinal cells or excessive gliosis/fibrosis, as both would interfere with the retinal-prosthesis interface. We have shown that a functional connection that requires synaptic transmission within the inner retina drives PVA evoked responses in the superior colliculus (Fransen et al., 2014). Here we show that the morphological basis for this connectivity is an intact inner retina in subretinally-implanted m- and bPVA devices. In addition, we show that morphology is maintained in two RP rat models, one with direct photoreceptor degeneration, the other with RPE dysfunction induced photoreceptor degeneration. This indicates that the effect we observe is general. We assessed rod bipolar cells because they represent the primary transmission pathway from the PVA to the RGCs and cholinergic amacrine cells because they are one of the most numerous amacrine cells and their processes form well known sublaminae in the the IPL. Together the two measures provide a

general assessment of inner retinal cell organization. While it is well-established that the degenerating retina undergoes remodeling when all photoreceptors are lost (Gargini et al., 2007; Marc et al., 2003; Strettoi et al., 2002), we show that in these models, rod bipolar cells and cholinergic amacrine cells within the implant site continue to exhibit typical and well-preserved morphology. Both their somata and processes within the IPL show normal localization and lamination. Previous studies show that normal retinas respond to both acute epiretinal electrical stimulation (Ray et al., 2009; Ray et al., 2011), or chronic subretinal implantation (Chow et al., 2001; Pardue et al., 2001; Tamaki et al., 2008; Yu et al., 2009) with an upregulation of GFAP expression and degenerative changes to the dendrites of rod bipolar cells. One study in which photosensitive dye-coupled film was subretinally implanted into RCS rat eyes showed preservation within the implant site of rod bipolar cell morphology via PKCα labeling (Alamusi et al., 2013), consistent with the findings we report here.

The increase in GFAP labeling in all unimplanted RCS and S334ter-3 retinas compared to WT (images not shown) is consistent with previous reports on retinal remodeling during degeneration (Marc and Jones, 2003; Zhao et al., 2012). Importantly, GFAP labeling in and around the implant site was similar to distal areas, suggesting that the glial reaction was not augmented by the presence of the PVA. Previous immunohistochemical studies of subretinal implants in animals with normal retinas have shown an increase in GFAP expression within the implant site (Chow et al., 2001; Pardue et al., 2001; Tamaki et al., 2008; Yu et al., 2009). It is feasible that any upregulation in GFAP due to implantation is masked when extensive gliosis due to photoreceptor degeneration is already present. Quantification of GFAP immunofluorescence showed a significant decrease in S334ter-3 retinas implanted with bPVAs compared to mPVAs. This may indicate that the gap design of the bPVA is more biocompatible with the retina and reduces the stress response. As the PVA devices are active and present electrical current to the underlying inner retina in response to light, it is possible that GFAP

339 expression in the Müller glia is tempered by neuroprotective effects of subretinal electrical
340 stimulation, which have been characterized previously (Ciavatta et al., 2013; Pardue et al.,
341 2005a; Pardue et al., 2005b).

342 The persistence of inner retinal cells and their intact organization under the implanted
343 device are consistent with our finding that PVA evoked responses are retained in the superior
344 colliculus and require inner retinal synaptic transmission (Fransen et al., 2014). Structural
345 integrity is critical to the success of function using this subretinal approach to visual restoration.
346 The presence of normal IPL sublamination suggests that other circuits that modulate the
347 excitatory signal are retained and may provide even better RGC and central signals. When
348 translated to the clinic, implantation will be performed at mid to late stage of photoreceptor
349 degeneration, similar to the implantation stages used here in the RCS and S334ter-3 rats,
350 respectively. The morphology of the retina implanted with both PVAs was similar, which also is
351 consistent with the functional results (Fransen et al., 2014) suggesting good compatibility at
352 both stages of degeneration.

353 The development of the next-generation bPVA is intended to improve upon the design of
354 the mPVA device, which has already been implanted in human patients (Chow et al., 2010;
355 Chow et al., 2004). Bipolar design of the pixel electrodes provides much tighter confinement of
356 electric field, and appears to improve spatial resolution, compared to monopolar arrangement in
357 mPVAs (Fransen et al., 2014). Our comparisons between mPVA- and bPVA-implanted retinas
358 and the reduced glial reaction in the retinas implanted with the bPVA device with the gaps
359 between pixels suggests improved biocompatibility and may indicate a longer duration of the
360 interface between the device and the retina, which needs to be tested empirically.

361 **5. Conclusions**

We found that both mPVA and bPVA devices implanted into the subretinal space were well tolerated by the inner retina in two rat models of RP with regard to rod bipolar, cholinergic amacrine, and Müller cell morphology. This initial analysis could be complemented with assays of other cell types (such as cone bipolar cells, horizontal cells as well as other amacrine cell classes). Other functional analyses could be aimed at examining the RGC responses and the timing and spatial distribution of their excitatory and inhibitory inputs. With our findings this would provide a complete understanding of the morphological and functional status of the inner retina in contact with the prosthesis.

Acknowledgements

Funding was provided by the National Institutes of Health (R01-EY-018608), the Air Force Office of Scientific Research (FA9550-04), NIH CTSA (UL1 RR025744, Stanford Spectrum fund) and a Stanford Bio-X IIP grant. K.M. was supported by an SU2P fellowship as part of an RCUK Science Bridges award. J.F. was supported by an NIH T32 grant (5 T32 HL 76138-09). M.P. was supported by a Research Career Scientist Award from the Department of Veterans Affairs.

Table 1: Primary antibodies used in this study to characterize inner retinal health.

Antigen	Antiserum	Source	Working Dilution	Cellular Target
PKCα	Polyclonal rabbit anti-PKCα	Santa Cruz Biotechnology, Inc., Dallas, TX	1:2000	Rod bipolar cells
GFAP	Polyclonal rabbit anti-GFAP	Abcam, Cambridge, MA	1:500	Glial reaction in retinal Müller cells
ChAT	Polyclonal goat anti-ChAT	Millipore, Billerica, MA	1:100	Cholinergic amacrine cells

Figures Captions

Figure 1. A) Sample fundus image of an RCS rat eye implanted subretinally with an mPVA. White dotted line indicates location of the cut made in the superior to inferior plane bisecting the posterior eye cup into implanted and non-implanted halves. “Implanted” region is indicated by the blue line. The area immediately “adjacent” to the implant site is shown by the red line. The green line displays an area opposite the implant within the non-implanted half, referred to as a “distal” area. The implant is 1mm in diameter. PKCα labeling in retinal cross-sections from WT rats (B), unimplanted control RCS rats at 2 months of age (F), RCS rats implanted from 4 to 8 weeks postnatal with a bPVA (C-E) and or mPVA (G-I). Rod bipolar cells are present with well-preserved morphology and localization at the implant site (C and G) relative to adjacent (D and H) and distal (E and I) regions. Implanted eyes show PKCα labeling consistent with that of age-matched unimplanted RCS controls (F). Wild-type retinas (B) appear to exhibit more intact dendritic tufts, but somata and axon terminal localization is comparable to that in RCS tissue. Insets 1B, 1C, 1 F & 1G show magnified images of the dendritic tufts in the OPL. ONL=outer nuclear layer, OPL=outer plexiform layer, INL=inner nuclear layer, IPL=inner plexiform layer, GCL=ganglion cell layer. Scale bar=50μm.

Figure 2. PKCα labeling in retinal cross-sections from S334ter-3 rats implanted with a bPVA (B-D, implanted from 7 to 27 weeks postnatal) or mPVA (F-H, implanted from 6 to 27 weeks postnatal). Implanted sections (B and F) show rod bipolar cell morphology that is comparable to that in adjacent (C and G) and distal (D and H) areas. The morphology and localization of these sections is consistent with that seen in age-matched unimplanted S334ter-3 controls (E). However, all S334ter-3 tissues exhibit virtually complete loss of the ONL and rod bipolar cell dendrites, both of which are still evident in wild-type retina (A). Scale bar=50μm.

Figure 3. PKCα, GFAP, and ChAT labeling quantification. The relative length of PKCα-labeled bipolar cells (A) did not show significant differences between retinal region or implant types. The

intensity of GFAP immunoreactivity (B) did not show significant differences between the retinal location within each implant type, but did show a difference between implant types (Two-way repeated ANOVA, $F(1, 15) = 14.38$ $p = 0.02$, $n = 6$). Immunoreactivity was normalized to the distal position for the PKCα and GFAP labeling. ChAT immunoreactive cell counts did not show significant differences between retinal location or implant type for either INL placed (C) or displaced (D) cholinergic amacrine cells. Error bars represent standard error of the mean.

Figure 4. ChAT labeling in retinal cross-sections from RCS eyes (C-E, implanted from 4 to 8 weeks postnatal) and S334ter-3 eyes (G-I, implanted from 7 to 27 weeks postnatal) with bPVA devices. Both RCS (B-E) and S334ter-3 sections (F-I), like wild-type (A), show typical cholinergic amacrine cell morphology with somata in the INL and GCL and processes in a dual-lamination pattern within the IPL. ChAT labeling patterns in implanted areas (C and G) are identical to those in adjacent (D and H), distal (E and I), Scale bar=50μm.

Figure 5. ChAT-labeled retinal flat mounts from RCS rats implanted from 4 to 8 weeks postnatal with an mPVA device (C and D) compared to unimplanted control eyes (A and B). *En face* view of control INL placed (A) and implanted INL placed (C) ChAT positive amacrine cells shows similar cholinergic amacrine cell distribution with consistent density. Similarly, labelling patterns of ChAT positive amacrine cells in the ganglion cell layer were consistent between control (B) and implanted (D) retinas. Scale bar=50μm.

Figure 6. GFAP labeling in retinal cross-sections from RCS (B-D) with bPVA and S334ter-3 eyes with mPVA (F-H) and bPVA (K-L) devices. RCS were implanted 4 to 8 weeks postnatally, while the S334ter-3 animals were implanted at 12 to 32 weeks. Glial reaction is widespread in all RCS tissue (A-D), but implanted areas (B) do not show increased GFAP labeling in comparison with adjacent (C), distal (D), and age-matched unimplanted control (A) sections. Similar to RCS tissue, S334ter-3 sections (E-L) show widespread gliosis due to photoreceptor

degeneration. However, GFAP labeling is not augmented in implanted regions (F and J) relative to adjacent (G and K), distal (H and L), and age-matched unimplanted control section (E). S334ter-3 retinas display a characteristic glial seal above the INL, not seen in wild-type retinas (data not shown), consistent with advanced photoreceptor degeneration. NFL=nerve fiber layer. Scale bar=50μm.

References

Adkins, A., Wang, W., Kaplan, H., Emery, D., Fernandez de Castro, J., Lee, S.-J., Huie, P., Palanker, D., McCall, M., Pardue, M., 2013. Morphological comparisons of flat and 3-dimensional subretinal photovoltaic arrays in rat and pig models of retinitis pigmentosa. Invest. Ophthalmol. Vis. Sci. 54, 1038.

Alamusi, Matsuo, T., Hosoya, O., Tsutsui, K.M., Uchida, T., 2013. Behavior tests and immunohistochemical retinal response analyses in RCS rats with subretinal implantation of Okayama-University-type retinal prosthesis. J. Artif. Organs 16, 343-351.

Asher, A., Segal, W.A., Baccus, S.A., Yaroslavsky, L.P., Palanker, D.V., 2007. Image processing for a high-resolution optoelectronic retinal prosthesis. IEEE Trans. Biomed. Eng. 54, 993-1004.

Bernstein, S.L., Guo, Y., 2011. Changes in cholinergic amacrine cells after rodent anterior ischemic optic neuropathy (rAION). Invest. Ophthalmol. Vis. Sci. 52, 904-910.

Bi, A.D., Cui, J.J., Ma, Y.P., Olshevskaya, E., Pu, M.L., Dizhoor, A.M., Pan, Z.H., 2006. Ectopic expression of a microbial-type rhodopsin restores visual responses in mice with photoreceptor degeneration. Neuron 50, 23-33.

Bringmann, A., Pannicke, T., Grosche, J., Francke, M., Wiedemann, P., Skatchkov, S.N., Osborne, N.N., Reichenbach, A., 2006. Muller cells in the healthy and diseased retina. Prog. Retin. Eye Res. 25, 397-424.

Busskamp, V., Picaud, S., Sahel, J.A., Roska, B., 2012. Optogenetic therapy for retinitis pigmentosa. Gene Ther. 19, 169-175.

Chow, A.Y., Bittner, A.K., Pardue, M.T., 2010. The artificial silicon retina in retinitis pigmentosa patients (an American Ophthalmological Association thesis). Trans. of the Am. Ophthalmol. Soc. 108, 120-154.

Chow, A.Y., Chow, V.Y., Packo, K.H., Pollack, J.S., Peyman, G.A., Schuchard, R., 2004. The artificial silicon retina microchip for the treatment of vision loss from retinitis pigmentosa. Arch. Ophthalmol. 122, 460-469.

Chow, A.Y., Pardue, M.T., Chow, V.Y., Peyman, G.A., Liang, C., Perlman, J.I., Peachey, N.S., 2001. Implantation of silicon chip microphotodiode arrays into the cat subretinal space. IEEE Trans. Neural Syst. Rehabil. Eng. 9, 86-95.

Ciavatta, V.T., Mocko, J.A., Kim, M.K., Pardue, M.T., 2013. Subretinal electrical stimulation preserves inner retinal function in RCS rat retina. Mol. Vis. 19, 995-1005.

Cicione, R., Shivdasani, M.N., Fallon, J.B., Luu, C.D., Allen, P.J., Rathbone, G.D., Shepherd, R.K., Williams, C.E., 2012. Visual cortex responses to suprachoroidal electrical stimulation of the retina: effects of electrode return configuration. J. Neural Eng. 9, 036009.

Dijk, F., Kamphuis, W., 2004. An immunocytochemical study on specific amacrine cell subpopulations in the rat retina after ischemia. Brain Res. 1026, 205-217.

Fransen, J. W., Pangeni, G., Pardue, M.T., McCall, M.A. 2014. Local signaling from a retinal prosthetic in a rodent retinitis pigmentosa model in vivo. J. Neural Eng. 11, 046012.

Garg, S.J., Federman, J., 2013. Optogenetics, visual prosthesis and electrostimulation for retinal dystrophies. Curr. Opin. Ophthalmol. 24, 407-414.

Gargini, C., Terzibasi, E., Mazzoni, F., Strettoi, E., 2007. Retinal organization in the retinal degeneration 10 (rd10) mutant mouse: a morphological and ERG study. J. Comp. Neurol. 500, 222-238.

Grünert, U., Martin ,P.R.,1991. Rod bipolar cells in the macaque monkey retina: immunoreactivity and connectivity. J Neurosci. 11, 2742-2758.

Hartong, D.T., Berson, E.L., Dryja, T.P., 2006. Retinitis pigmentosa. Lancet 368, 1795-1809.

Humayun, M.S., Dorn, J.D., da Cruz, L., Dagnelie, G., Sahel, J.A., Stanga, P.E., Cideciyan, A.V., Duncan, J.L., Eliott, D., Filley, E., Ho, A.C., Santos, A., Safran, A.B., Arditi, A., Del

506 Priore, L.V., Greenberg, R.J., Argus, I.I.S.G., 2012. Interim results from the international
507 trial of Second Sight's visual prosthesis. Ophthalmology 119, 779-788.
508 Humayun, M.S., Prince, M., de Juan, E., Barron, Y., Moskowitz, M., Klock, I.B., Milam, A.H.,
509 1999. Morphometric analysis of the extramacular retina from postmortem eyes with
510 retinitis pigmentosa. Invest. Ophthalmol. Vis. Sci. 40, 143-148.
511 Isago, H., Sugano, E., Wang, Z., Murayama, N., Koyanagi, E., Tamai, M., Tomita, H., 2012.
512 Age-Dependent Differences in Recovered Visual Responses in Royal College of
513 Surgeons Rats Transduced with the Channelrhodopsin-2 Gene. J. of Mol. Neurosci. 46,
514 393-400.
515 Jensen, R.J., Ziv, O.R., Rizzo, J.F., 2005. Responses of rabbit retinal ganglion cells to electrical
516 stimulation with an epiretinal electrode. J. Neural Eng. 2, S16-21.
517 Jones, B.W., Watt, C.B., Frederick, J.M., Baehr, W., Chen, C.K., Levine, E.M., Milam, A.H.,
518 Lavail, M.M., Marc, R.E., 2003. Retinal remodeling triggered by photoreceptor
519 degenerations. J. Comp. Neurol. 464, 1-16.
520 Jones, B.W., Marc, R.E., 2005. Retinal remodeling during retinal degeneration. Exp. Eye Res.
521 81, 123-137.
522 Kanda, H., Morimoto, T., Fujikado, T., Tano, Y., Fukuda, Y., Sawai, H., 2004.
523 Electrophysiological studies of the feasibility of suprachoroidal-transretinal stimulation for
524 artificial vision in normal and RCS rats. Invest. Ophthalmol. Vis. Sci. 45, 560-566.
525 Kosaka, J., Suzuki, A., Morii, E., Nomura, S., 1998. Differential localization and expression of
526 alpha and beta isoenzymes of protein kinase C in the rat retina. J. Neurosci. Res. 54,
527 655-663.
528 LaVail, M.M., Battelle, B.A., 1975. Influence of eye pigmentation and light deprivation on
529 inherited retinal dystrophy in the rat. Exp. Eye Res. 21, 167-192.
530 LaVail, M.M., Sidman, R.L., Gerhardt, C.O., 1975. Congenic strains of RCS rats with inherited
531 retinal dystrophy. J. Hered. 66, 242-244.

Lee, E.J., Padilla, M., Merwine, D.K., Grzywacz, N.M., 2008. Developmental regulation of the morphology of mouse retinal horizontal cells by visual experience. Eur. J. Neurosci. 27, 1423-1431.

Lin, B., Koizumi, A., Tanaka, N., Panda, S., Masland, R.H., 2008. Restoration of visual function in retinal degeneration mice by ectopic expression of melanopsin. Proc. Natl. Acad. Sci. U.S.A. 105, 16009-16014.

Mandel, Y., Goetz, G., Lavinsky, D., Huie, P., Mathieson, K., Wang, L., Kamins, T., Galambos, L., Manivanh, R., Harris, J., Palanker, D., 2013. Cortical responses elicited by photovoltaic subretinal prostheses exhibit similarities to visually evoked potentials. Nat. Commun. 4, 1980.

Marc, R.E., Jones, B.W., 2003. Retinal remodeling in inherited photoreceptor degenerations. Mol. Neurobiol. 28, 139-147.

Marc, R.E., Jones, B.W., Anderson, J.R., Kinard, K., Marshak, D.W., Wilson, J.H., Wensel, T., Lucas, R.J., 2007. Neural reprogramming in retinal degeneration. Invest. Ophthalmol. Vis. Sci. 48, 3364-3371.

Marc, R.E., Jones, B.W., Watt, C.B., Strettoi, E., 2003. Neural remodeling in retinal degeneration. Prog. Retin. Eye Res. 22, 607-655.

Mathieson, K., Loudin, J., Goetz, G., Huie, P., Wang, L., Kamins, T.I., Galambos, L., Smith, R., Harris, J.S., Sher, A., Palanker, D., 2012. Photovoltaic Retinal Prosthesis with High Pixel Density. Nat. Photonics 6, 391-397.

McGill, T.J., Prusky, G.T., Douglas, R.M., Yasumura, D., Matthes, M.T., Lowe, R.J., Duncan, J.L., Yang, H., Ahern, K., Daniello, K.M., Silver, B., LaVail, M.M., 2012. Discordant anatomical, electrophysiological, and visual behavioral profiles of retinal degeneration in rat models of retinal degenerative disease. Invest. Ophthalmol. Vis. Sci. 53, 6232-6244.

Morimoto, T., Kamei, M., Nishida, K., Sakaguchi, H., Kanda, H., Ikuno, Y., Kishima, H., Maruo, T., Konoma, K., Ozawa, M., Nishida, K., Fujikado, T., 2011. Chronic Implantation of

Newly Developed Suprachoroidal-Transretinal Stimulation Prosthesis in Dogs. Invest. Ophthalmol. Vis. Sci. 52, 6785-6792.

Mullen, R.J., LaVail, M.M., 1976. Inherited retinal dystrophy: primary defect in pigment epithelium determined with experimental rat chimeras. Science 192, 799-801.

O'Brien, E.E., Greferath, U., Vessey, K.A., Jobling, A.I., Fletcher, E.L., 2012. Electronic restoration of vision in those with photoreceptor degenerations. Clin. Exp. Optom. 95, 473-483.

Palanker, D., Huie, P., Vankov, A., Aramant, R., Seiler, M., Fishman, H., Marmor, M., Blumenkranz, M., 2004. Migration of retinal cells through a perforated membrane: implications for a high-resolution prosthesis. Invest. Ophthalmol. Vis. Sci. 45, 3266-3270.

Pardue, M.T., Phillips, M.J., Yin, H., Fernandes, A., Cheng, Y., Chow, A.Y., Ball, S.L., 2005a. Possible sources of neuroprotection following subretinal silicon chip implantation in RCS rats. J. Neural Eng. 2, S39-47.

Pardue, M.T., Phillips, M.J., Yin, H., Sippy, B.D., Webb-Wood, S., Chow, A.Y., Ball, S.L., 2005b. Neuroprotective effect of subretinal implants in the RCS rat. Invest. Ophthalmol. Vis. Sci. 46, 674-682.

Pardue, M.T., Stubbs, E.B., Jr., Perlman, J.I., Narfstrom, K., Chow, A.Y., Peachey, N.S., 2001. Immunohistochemical studies of the retina following long-term implantation with subretinal microphotodiode arrays. Exp. Eye Res. 73, 333-343.

Ray, A., Colodetti, L., Weiland, J.D., Hinton, D.R., Humayun, M.S., Lee, E.J., 2009. Immunocytochemical analysis of retinal neurons under electrical stimulation. Brain Res. 1255, 89-97.

Ray, A., Lee, E.J., Humayun, M.S., Weiland, J.D., 2011. Continuous electrical stimulation decreases retinal excitability but does not alter retinal morphology. J. Neural Eng. 8, 045003.

583 Rizzo, J.F., 3rd, 2011. Update on retinal prosthetic research: the Boston Retinal Implant Project.
584 J. Neuroophthalmol. 31, 160-168.
585 Strettoi, E., Porciatti, V., Falsini, B., Pignatelli, V., Rossi, C., 2002. Morphological and functional
586 abnormalities in the inner retina of the rd/rd mouse. J. Neurosci. 22, 5492-5504.
587 Strettoi, E., Pignatelli, V., Rossi, C., Porciatti, V., Falsini, B., 2003. Remodeling of second-order
588 neurons in the retina of rd/rd mutant mice. Vision Research 43, 867–877.

589 Tamaki, T., Matsuo, T., Hosoya, O., Tsutsui, K.M., Uchida, T., Okamoto, K., Uji, A., Ohtsuki, H.,
590 2008. Glial reaction to photoelectric dye-based retinal prostheses implanted in the
591 subretinal space of rats. J. Artif. Organs 11, 38-44.
592 Tomita, H., Sugano, E., Yawo, H., Ishizuka, T., Isago, H., Narikawa, S., Kugler, S., Tamai, M.,
593 2007. Restoration of visual response in aged dystrophic RCS rats using AAV-mediated
594 channelopsin-2 gene transfer. Invest. Ophthalmol. Vis. Sci. 48, 3821-3826.
595 Uji, A., Matsuo, T., Ishimaru, S., Kajiura, A., Shimamura, K., Ohtsuki, H., Dan-oh, Y., Suga, S.,
596 2005. Photoelectric dye-coupled polyethylene film as a prototype of retinal prostheses.
597 Artif. Organs 29, 53-57.
598 Wang, L., Mathieson, K., Kamins, T.I., Loudin, J.D., Galambos, L., Goetz, G., Sher, A., Mandel,
599 Y., Huie, P., Lavinsky, D., Harris, J.S., Palanker, D.V., 2012. Photovoltaic retinal
600 prosthesis: implant fabrication and performance. J. Neural Eng. 9, 046014.
601 Wong, Y.T., Chen, S.C., Seo, J.M., Morley, J.W., Lovell, N.H., Suaning, G.J., 2009. Focal
602 activation of the feline retina via a suprachoroidal electrode array. Vis. Res. 49, 825-833.
603 Yamauchi, Y., Franco, L.M., Jackson, D.J., Naber, J.F., Ziv, R.O., Rizzo, J.F., Kaplan, H.J.,
604 Enzmann, V., 2005. Comparison of electrically evoked cortical potential thresholds
605 generated with subretinal or suprachoroidal placement of a microelectrode array in the
606 rabbit. J. Neural Eng. 2, S48-56.

Yu, W., Wang, X., Zhao, C., Yang, Z., Dai, R., Dong, F., 2009. Biocompatibility of subretinal parylene-based Ti/Pt microelectrode array in rabbit for further artificial vision studies. J. Ocul. Biol. Dis. Infor. 2, 33-36.

Zhao, T., Li, Y., Weng, C., Yin, Z., 2012. The changes of potassium currents in RCS rat Muller cell during retinal degeneration. Brain Res. 1427, 78-87.

Zrenner, E., Stett, A., Weiss, S., Aramant, R.B., Guenther, E., Kohler, K., Miliczek, K.D., Seiler, M.J., Haemmerle, H., 1999. Can subretinal microphotodiodes successfully replace degenerated photoreceptors? Vis. Res. 39, 2555-2567.

Figure(s)

Click here to download high resolution image

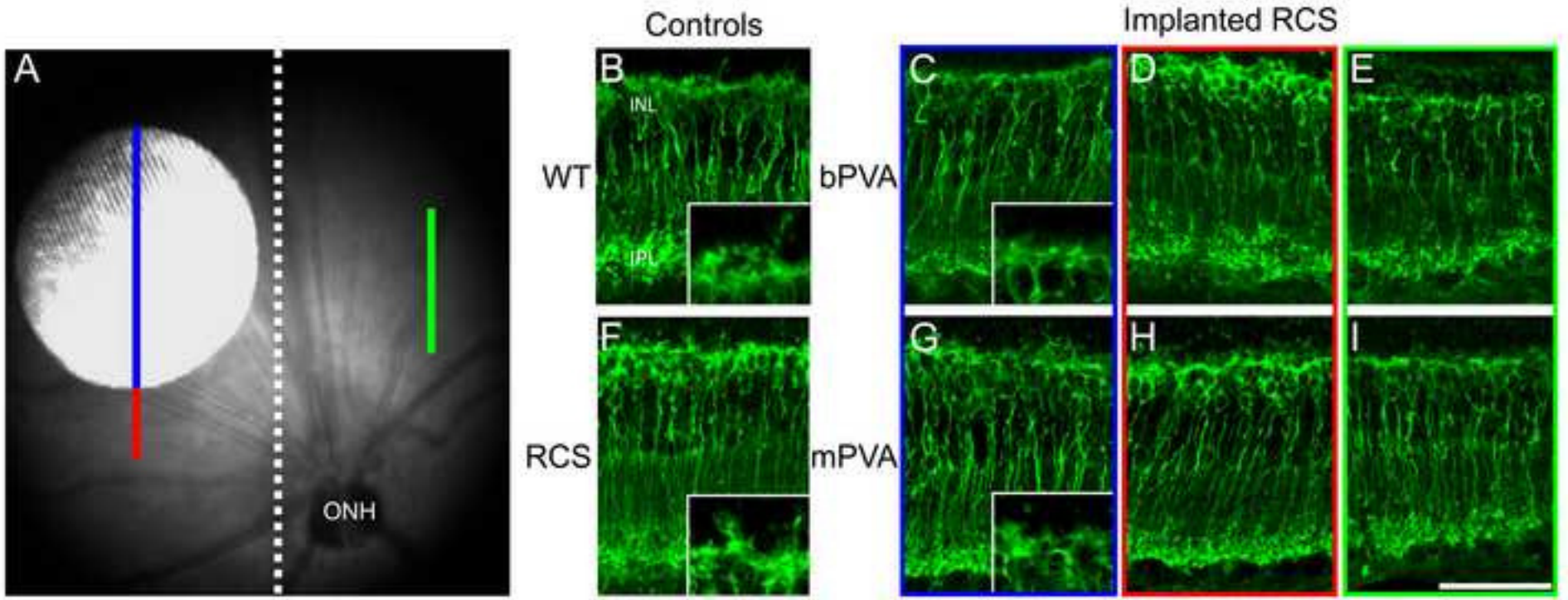

Figure(s)

Click here to download high resolution image

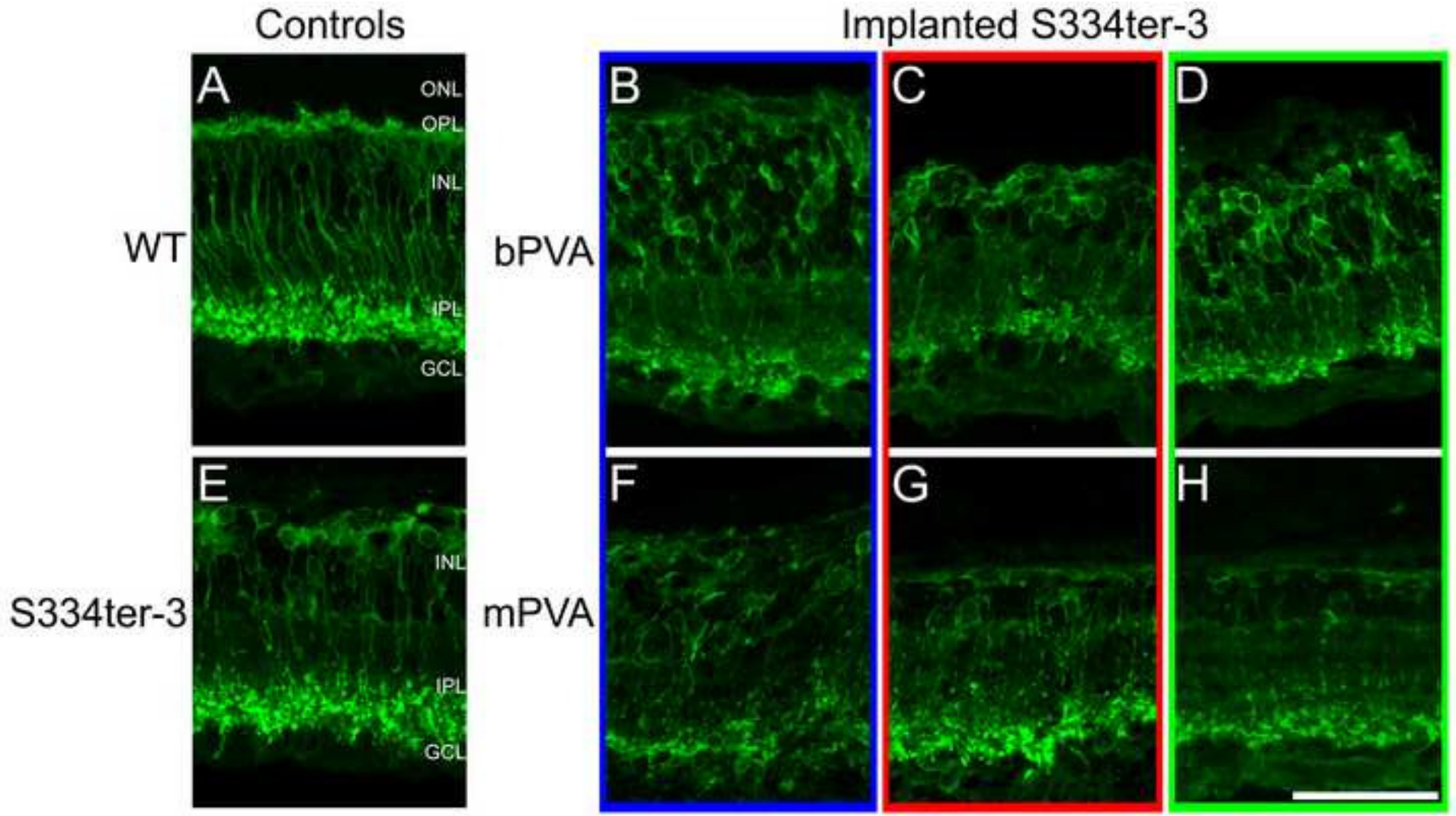

Figure(s)

Click here to download high resolution image

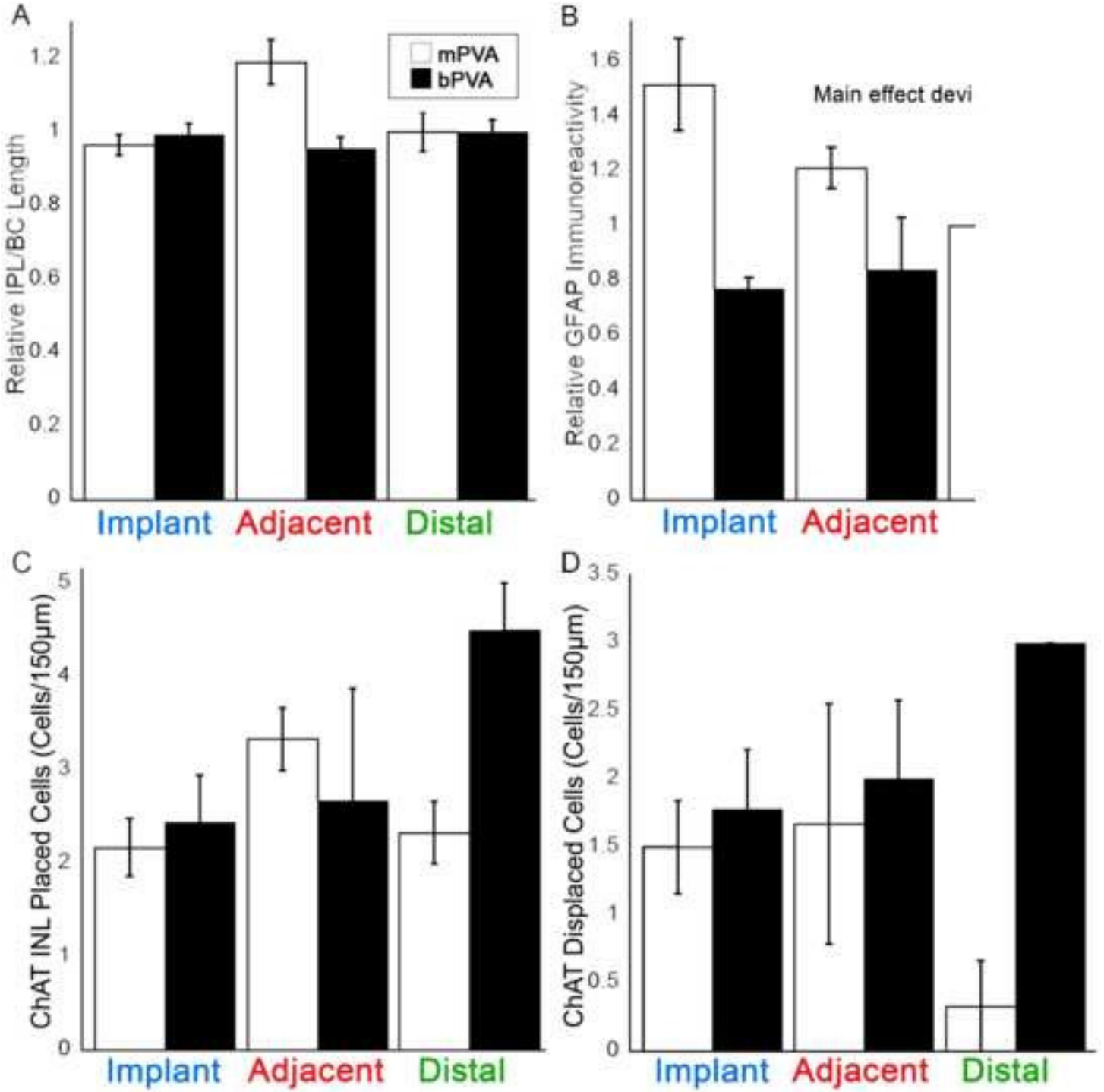

Figure(s)

Click here to download high resolution image

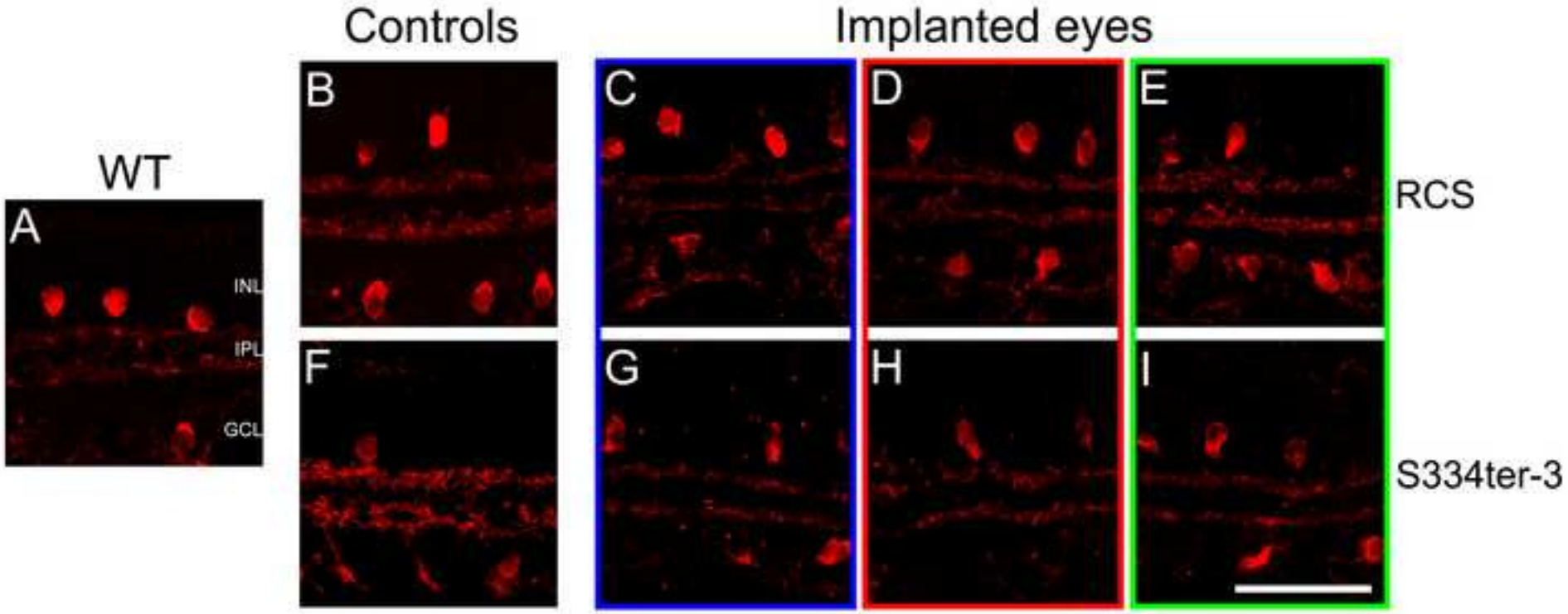

Figure(s)
Click here to download high resolution image

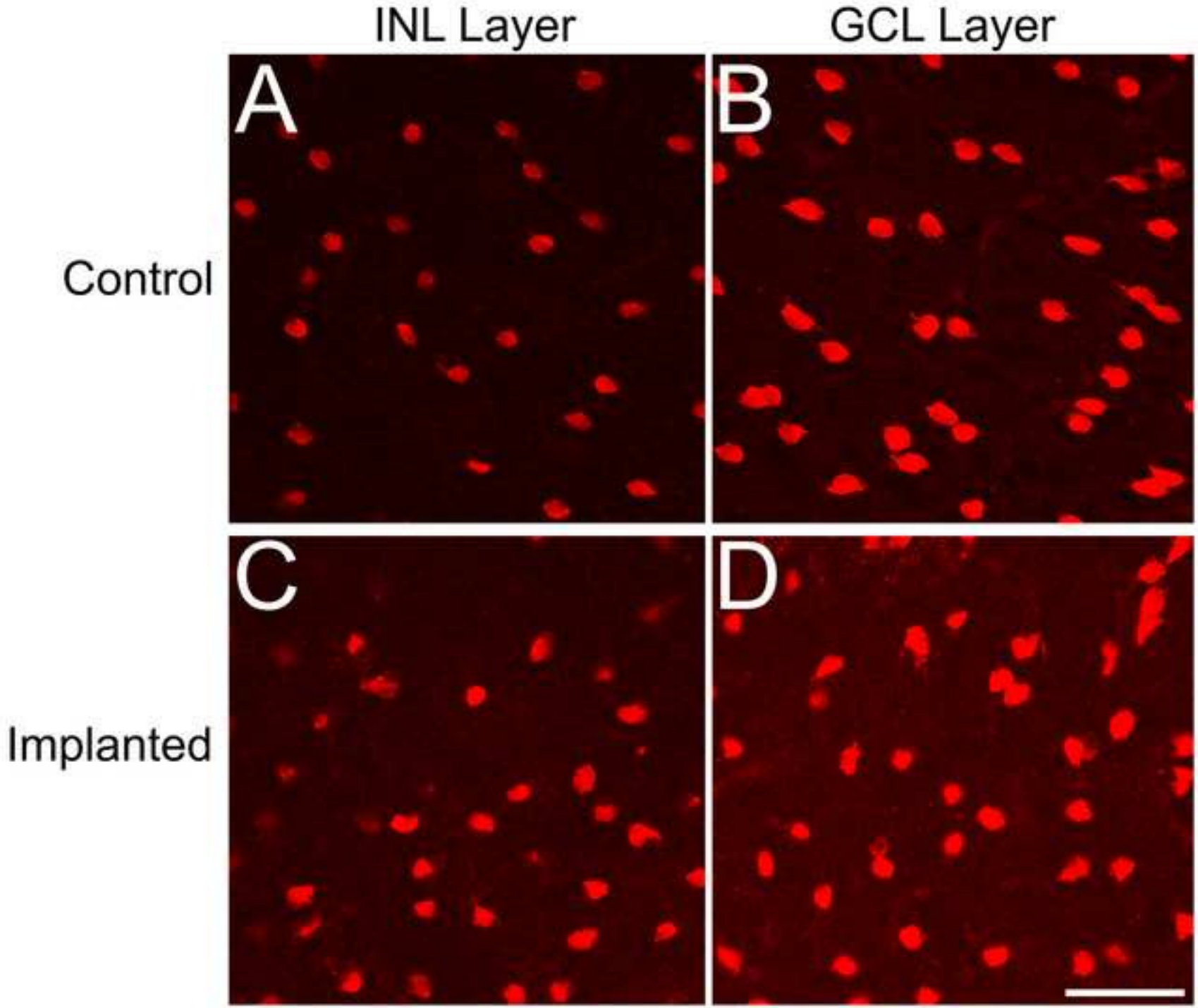

Figure(s)

Click here to download high resolution image